

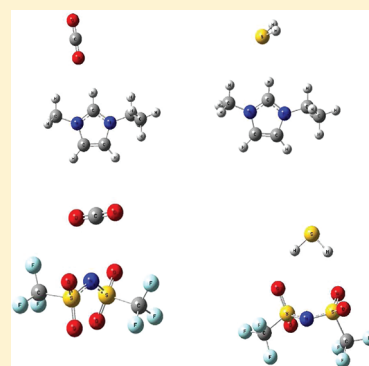
Solubility of CO₂, H₂S, and Their Mixture in the Ionic Liquid 1-Octyl-3-methylimidazolium Bis(trifluoromethyl)sulfonylimide

Amir Hossein Jalili,^{*,†} Mohammadali Safavi,[‡] Cyrus Ghotbi,[‡] Ali Mehdizadeh,[†] Masih Hosseini-Jenab,[†] and Vahid Taghikhani[‡]

[†]Gas Science Department, Gas Research Division, Research Institute of Petroleum Industry (RIPI), P.O. Box 14665-137, West Blvd., Azadi Sport Complex, Tehran, Iran

[‡]Department of Chemical and Petroleum Engineering, Sharif University of Technology, Azadi Ave., Tehran, Iran

ABSTRACT: Gaseous solubilities of carbon dioxide (1), hydrogen sulfide (2), and their binary mixture ($x_2 \approx 0.2, 0.5, 0.8$) have been measured in the ionic liquid 1-octyl-3-methylimidazolium bis(trifluoromethyl)sulfonylimide ($[\text{C}_8\text{mim}][\text{Tf}_2\text{N}]$) at temperatures ranging from (303.15 to 353.15) K and at pressures under 2 MPa. The observed PTx solubility data were used to obtain Henry's law constants and correlated by three models: (1) the simple Krichevsky–Kasarnovsky (KK) equation, (2) a model comprised of the extended Henry's law and the Pitzer's virial expansion for the excess Gibbs free energy, and (3) the generic Redlich–Kwong (RK) cubic equation of state proposed for gas–ionic liquid systems. The correlations from the three models show quite good consistency with the experimental data for IL/CO₂ and IL/H₂S binary mixtures within experimental uncertainties. For IL/CO₂/H₂S ternary mixtures, the RK model shows the best correlation with the experimental data. The comparison showed that the solubility of H₂S is about two times as great as that of CO₂ in the ionic liquid studied in this work. It was further found, by comparison of the experimental data of this study with those of previous reports, that the solubility of H₂S in $[\text{C}_n\text{mim}][\text{Tf}_2\text{N}]$ ILs increases as the number of carbon atoms in the alkyl substituent of methylimidazolium cation, n , increases. In addition, quantum chemical calculations at DFT/B3LYP level of theory using 6-311+G(d) and 6-311++G(2d,2p) basis sets were performed on the isolated systems studied in this work to provide explanations from a molecular point of view for the observed experimental trends.



INTRODUCTION

Room temperature ionic liquids (RTILs), also known as liquid salts, ionic melts, and liquid electrolytes, have emerged as an important family of organic compounds since 1995.¹ Due to their tunable chemical structures, they show various promising applications such as gas storage, separation, and catalysis. This class of compounds are comprised of an organic cation like quaternary ammonium, imidazolium, and pyridinium ions and an inorganic or organic anion such as $[\text{Cl}]^-$, $[\text{BF}_4]^-$, $[\text{PF}_6]^-$, or $[\text{Tf}_2\text{N}]^-$ and are molten salts, which are liquid over a wide temperature range including ambient temperature (below the boiling point of water).¹ Due to the existence of Coulombic attraction between the ions of ILs, they exhibit negligibly small vapor pressure, meaning that ionic liquids are essentially nonvolatile and could facilitate the absorption of gases without loss of the capture agent into the gas stream. They also have high thermal and electrochemical stability.

Nowadays, given the tendency for green processes and sustainable technology, one of the active research areas is exploring ionic liquids as an alternative or even replacement to conventional alkanolamine solutions² for removal of acid gases (CO₂ and H₂S) in gas sweetening processes.^{3–7} Another research area is concerned with the fixation and sequestration of CO₂, which is regarded as the most important greenhouse gas by employing ionic liquids.⁸ Solubility and diffusion

coefficient data of acid gases (CO₂ and H₂S) at various temperatures and pressures are important in the evaluation of ionic liquids (ILs) for use in industrial natural gas treating as well as other industrially important processes. A growing number of experimental data for solubility and diffusion of CO₂ in various ILs have become available in the past few years, which in the case of $[\text{C}_8\text{mim}]^+$ -based ILs include the following: (1) the high-pressure phase equilibrium data presented by Blanchard et al.⁸ for CO₂ with six imidazolium-based ILs including $[\text{C}_8\text{mim}][\text{BF}_4]$ and $[\text{C}_8\text{mim}][\text{PF}_6]$ at temperatures of 313.15, 323.15, and 333.15 K and pressures of up to 9.6 MPa. The authors concluded that the volume expansion of liquid IL phase is negligible even for large amounts of dissolved CO₂ and also that the solubility of ILs in the CO₂ phase is exceedingly low; (2) subsequent high-pressure phase behavior of CO₂ in 10 different imidazolium-based ILs including $[\text{C}_8\text{mim}][\text{Tf}_2\text{N}]$ at temperatures of 298.15, 313.15, and 333.15 K and pressures up to 15 MPa, reported by Aki et al.⁹ In their investigation, the latter group concluded that the solubility of CO₂ is greater in ILs with anions having $-\text{CF}_3$ groups such as $[\text{Tf}_2\text{N}]^-$ and also that the solubility increases by increasing the alkyl group chain

Received: August 6, 2011

Revised: February 8, 2012

Published: February 28, 2012

length in the cation part of the IL; (3) Henry's law constant at 298.15 K, reported by Baltus et al.¹⁰ for CO₂ in [C₈mim][Tf₂N] as well as eight different imidazolium-based ILs from the low-pressure solubility data obtained by using a quartz crystal microbalance apparatus; (4) Henry's law constant due to Chen et al.¹¹ for the solubility of CO₂ in imidazolium-based tetrafluoroborate [BF₄]⁻ ILs at $T = 307.55, 312.45, 317.45,$ and 322.15 K. They concluded that the solubility increases by increasing the alkyl chain length of the imidazolium cation ring in the sequence: [C₈mim][BF₄] > [C₆mim][BF₄] > [C₄mim][BF₄]; (5) measurements made by Zhang et al.¹² for the solubility at infinite dilution of CO₂ in [C₈mim][BF₄] as well as a series of 1-butyronitrile substituted imidazolium-based ILs at $T = 303, 313,$ and 323 K by using the gas chromatography technique; (6) high-pressure phase behavior of CO₂ + [C₈mim][BF₄], which has been measured by Gutkowski et al.¹³ in the pressure and temperature range of 0.1–100 MPa and 303–363 K, respectively, 7) high-pressure solubility data of CO₂ in 1-alkyl-3-methylimidazolium bis(trifluoromethyl)sulfonylimide ([C_{*n*}mim][Tf₂N], $n = 2, 4, 6, 8$), reported by Shin et al.¹⁴ at pressures up to 45 MPa and temperatures between 298.15 and 343.15 K, and finally (8) subsequent high-pressure phase equilibrium data of carbon dioxide with 1-alkyl-3-methylimidazolium trifluoromethanesulfonate ([C_{*n*}mim][OTf], $n = 2, 4, 6, 8$) ILs at pressures up to 40 MPa and at temperatures between 303.85 and 344.55 K reported by Shin et al.¹⁵ The latter group used the Peng–Robinson equation of state to correlate the obtained experimental data. For hydrogen sulfide, however, experimental data for solubility and diffusion in ILs are not as versatile as those for carbon dioxide. Jou and Mather¹⁶ provided the first report regarding the solubility of H₂S in ILs, that is, 1-butyl-3-methylimidazolium hexafluorophosphate ([C₄mim][PF₆]) at temperatures from 298.15 to 403.15 K and pressures up to 9.6 MPa. Subsequently, Pomelli et al.¹⁷ reported the solubility of H₂S in different [C_{*n*}mim]⁺-based ILs with different anions and in a series of [Tf₂N]⁻ ILs with different cations at 298.15 K and 1400 kPa, using a medium pressure NMR technique. They observed that H₂S is stable with no sign of reaction under the investigated experimental conditions. Their quantum chemical calculations show that the interaction energy between H₂S and the anion part of the ILs is comparable in strength to that of traditional hydrogen bonds and concluded that this is the main factor responsible for the high solubility of hydrogen sulfide in ILs. Heintz et al.¹⁸ measured the solubility of CO₂ as well as a mixture of N₂/H₂S in a polymeric ammonium polyether-based IL with chloride anion in the temperature range from 300 to 500 K and pressures up to 0.23 and 3.0 MPa for H₂S and CO₂, respectively. Shiflett and Yokozeki¹⁹ reported the phase equilibrium VLE measurements of binary mixtures of H₂S and CO₂ with [C₄mim][PF₆] at temperatures from (273.6 to 342.2) K for H₂S and at $T = 283.1$ and 293.0 K for CO₂ and ternary mixture of H₂S/CO₂/[C₄mim][PF₆] at $T = 298.15$ and 333.15 K and pressures up to 6.5 MPa. The remaining data concerning the solubility of H₂S in ILs have been produced in our laboratory at temperatures ranging from 303.15 to 353.15 K and pressures up to about 2.0 MPa. This includes the solubility of H₂S in [C₄mim][PF₆], [C₄mim][BF₄], and [C₄mim][Tf₂N],²⁰ the solubility of H₂S in [C₆mim][PF₆], [C₆mim][BF₄], and [C₆mim][Tf₂N],²¹ the solubility and diffusion of H₂S and CO₂ in 1-(2-hydroxyethyl)-3-methylimidazolium tetrafluoroborate ([HOC₂mim][BF₄]),²² the solubility and diffusion of H₂S and CO₂ in 1-ethyl-3-methylimidazolium

ethylsulfate ([C₂mim][EtSO₄]),²³ and most recently the solubility of H₂S in [HOC₂mim]⁺-based ILs containing [PF₆]⁻, [OTf]⁻, and [Tf₂N]⁻ anions,²⁴ and [C₂mim]⁺-based ILs containing [PF₆]⁻ and [Tf₂N]⁻ anions.²⁵ All of the data obtained have been used to estimate Henry's law constants or diffusion coefficients at different temperatures.

We are interested in examining the potential of ILs for the separation of CO₂ and H₂S from natural gas and also for the separation of H₂S and CO₂ gases from each other in the gaseous streams containing them. The data reported by other researchers (mentioned above) for the CO₂–[C₈mim][Tf₂N] system except those of Baltus et al.¹⁰ at 298.15 K are mainly obtained at high pressures, which are neither of sufficient accuracy for extrapolation to low pressure regions nor for estimating the Henry's law constants at various temperatures. Also to our best knowledge, there is no reported solubility data for H₂S–[C₈mim][Tf₂N] system in the open literature. Thus, this paper focuses on solubility of CO₂ and H₂S in the ionic liquid [C₈mim][Tf₂N] in the low to medium pressure range (up to about 2.0 MPa) at temperatures from 303.15 to 353.15 K. This way we will have sufficient experimental data in addition to the ones previously reported for the other members and will be able to follow the solubility behavior of CO₂ and H₂S acid gases in [C_{*n*}mim][Tf₂N] ionic liquids. In addition, because of the inconsistency between the Henry's law constants at zero pressure for solubility of H₂S in [C₆mim][Tf₂N] reported in our previous work²¹ and the other members of [C_{*n*}mim][Tf₂N] family, the PTx data for H₂S/[C₆mim][Tf₂N] system were again measured in this study. The solubilities determined are used to estimate zero pressure Henry's law constants and partial molar thermodynamic functions of solution of H₂S and CO₂ at different temperatures. Correlation equations for the obtained Henry's law constants with temperature are presented here. Also the solubility of CO₂/H₂S mixtures in [C₈mim][Tf₂N] is investigated in this study to explore the facility of separation of these gases from each other in streams containing them. The notion behind this consideration is the large difference in Henry's law constants for the solubility of H₂S and CO₂ in the ionic liquids studied to date,^{19–25} which suggests that the selective capturing and separation of these gases may also be possible using [C₈mim][Tf₂N]. In the next step, the obtained solubility data are modeled by using two distinct correlation equations, that is, the extended Henry's law combined with Pitzer's activity coefficient model for electrolytes,^{26,27} which takes into account the nonideality of solute in liquid solvent through activity coefficients, and a generic Redlich–Kwong type equation of state proposed by Shiflett and Yokozeki for gas–ionic liquid systems.^{28–31} The two models are compared with each other and with the simple Krichevsky–Kasarnovsky equation,³² through comparison of the predicted results with that of experimental data. The experimental results obtained in this work are also compared with the corresponding data for [C₆mim][Tf₂N], [C₄mim][Tf₂N], and [C₂mim][Tf₂N] reported in the literature. Finally, ab initio density functional theory (DFT) quantum chemical calculations on the [C_{*n*}mim][Tf₂N] ionic liquids and their interaction with CO₂ and H₂S molecules were performed to understand the observed solubility behaviors investigated in this work.

EXPERIMENTAL METHODS

Materials. Carbon dioxide and hydrogen sulfide (c.p. grade 99.95% min) were obtained from Roham Gas Company.

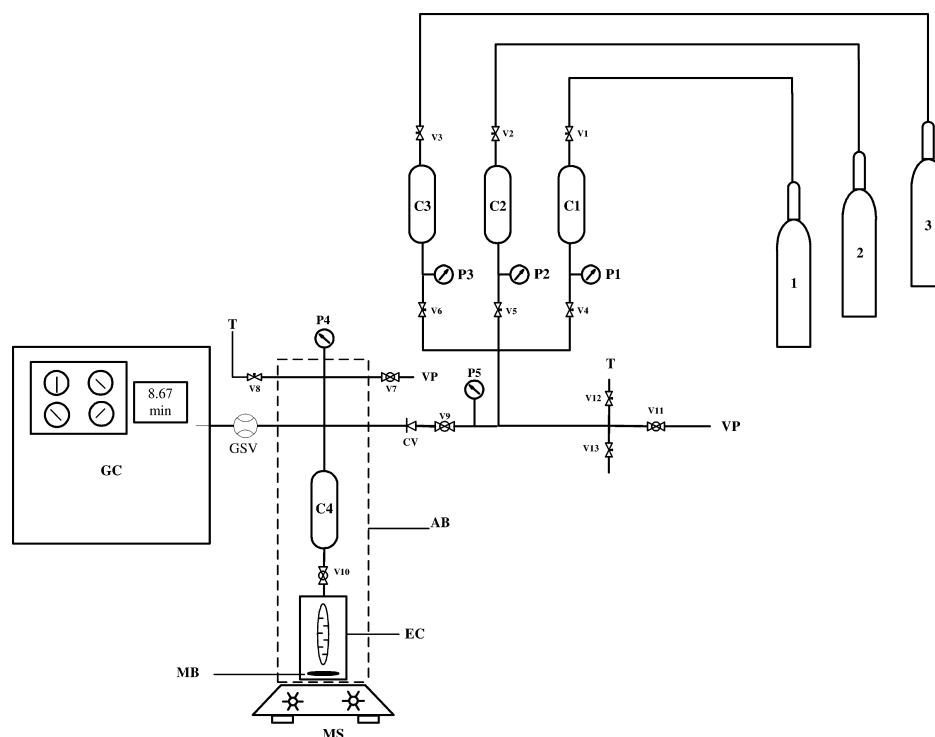


Figure 1. Apparatus for the measurement of the solubility of pure and mixtures of CO₂ and H₂S acid gases in liquids: 1, CO₂ gas cylinder; 2, H₂S gas cylinder; 3, He gas cylinder; C1–C3, CO₂, H₂S, and He gas containers, respectively; C4, gas mixture container; P1–P3, pressure sensors (transmitters); V1–V13, valves; CV, check valve; GSV, gas sampling valve; GC, gas chromatograph; AB, air bath; EC, equilibrium cell; MB, magnetic bar; MS, magnetic stirrer; VP, vacuum pump; T, trap (acid gas scrubber).

The ionic liquid [C₈mim][Tf₂N] was supplied by Merck Chemical Company with a nominal purity of >99%. [C₈mim][Tf₂N] was synthesized according to a known literature procedure.^{1,33} A mixture of 8.2 g (0.10 mol) of 1-methylimidazole (Merck, 99%) and 16.4 g (0.11 mol) of *n*-octyl chloride (Merck >98%) was refluxed for 29 h at 373 K. The reaction mixture was then washed with ethyl acetate to remove unreacted starting materials. The oily product obtained was then heated at 343 K for 7 h at reduced pressure to remove the residual water. A sample of 18.5 g of 1-octyl-3-methylimidazolium chloride ([C₈mim][Cl]) was obtained (80% yield). ¹H NMR (300 MHz, CDCl₃, 25 °C) δ (ppm) = 0.47 (3H, t, NCH₂(CH₂)₆CH₃), 0.89 (10H, m, NCH₂CH₂(CH₂)₅CH₃), 1.54 (2H, m, NCH₂CH₂(CH₂)₅CH₃), 3.75 (3H, s, NCH₃), 3.95 (2H, t, NCH₂(CH₂)₆CH₃), 7.27 (1H, d, H-4), 7.50 (1H, d, H-5), 10.12 (1H, s, H-2).

To a mixture of 18.5 g (0.08 mol) of 1-octyl-3-methylimidazolium chloride in 67 mL of deionized water, 25.8 g (0.09 mol) of lithium bis(trifluoromethyl)sulfonylimide (Merck >98%) was added at room temperature. The two-phase mixture obtained was magnetically stirred at room temperature for 24 h. Upon completion of the reaction, as monitored by thin layer chromatography (TLC), the IL was separated from the reaction mixture as a dense phase. The upper aqueous phase was washed with CH₂Cl₂ (2 × 20 mL). The washings were combined with the organic layer, and the latter was dried over anhydrous MgSO₄. After filtration, the solvent was removed using a rotary evaporator, and the product was then heated at reduced pressure for 7 h at 343 K to remove residual water. The yield was 90%. ¹H NMR (300 MHz, CDCl₃, 25 °C): δ (ppm) = 0.98 (3H, t, NCH₂(CH₂)₆CH₃), 1.40 (10H, m, NCH₂CH₂(CH₂)₅CH₃), 1.89 (2H, m, NCH₂CH₂(CH₂)₅CH₃), 3.97 (3H, s, NCH₃), 4.20 (2H, t, NCH₂(CH₂)₆CH₃), 7.34 (1H, d, H-4), 7.35 (1H, d, H-5), 8.77 (1H, s, H-2).

Apparatus and Procedure. The experimental apparatus of Jalili et al.²⁰ for the solubility of pure gases in ILs was modified to measure pure and mixed gas solubility. The experimental setup is shown schematically in Figure 1. It consists of a high-pressure equilibrium cell (EC) and three gas containers (C1 to C3) for introducing known amounts of CO₂, H₂S, and He into the gas mixture container (C4). All wetted compartments of the apparatus are constructed from stainless steel (SS 316 L). The equilibrium cell was equipped with a magnetic bar (MB) driven by a magnetic stirrer (MS) at the bottom of the cell to facilitate heat and mass transfer inside the cell. The equilibrium cell was connected through a ball valve (V10) to the gas mixture container (C4). The equilibrium cell and the gas mixture container were placed inside an air bath (AB), the temperature of which was controlled to within 0.05 K. The equilibrium temperature was measured with a Lutron model TM-917 digital thermometer with a 0.01 K resolution using a Pt-100 sensor inserted into the air bath (AB). The equilibrium cell and the gas container pressures were measured using a Keller model PA-33X pressure transmitter sensors in the range of 0–2 MPa, which were uncertain to within 0.01% of their full scale. The calibration of pressure sensors was carried out against a pneumatic dead-weight gauge (DH-Budenberg, model 550). The volumes of different compartments of the apparatus were measured using a calibrated bulb of known volume. First, the calibrated bulb was connected to the apparatus via valve 13 (Figure 1). The whole system was evacuated through valve 11, and then valve 13 was closed. The apparatus was pressurized to atmospheric pressure by opening valve 12 to atmospheric air, and the temperature was allowed to equilibrate. Using the ideal gas law, the volume of the system was calculated from the pressure drop when valve 13 was again opened while valve 12 was closed. The volume of the calibrated bulb was measured

within a tenth of a milliliter by filling the bulb with distilled water and then measuring the mass of the water by using an analytical balance (Mettler model AE 200) with an uncertainty ± 0.0001 g. The measured volume of the various parts of the apparatus was uncertain to within ± 0.5 mL. The composition of the gas phase, which was assumed to be solely composed of H_2S and CO_2 , was assessed by gas chromatography (GC). The vapor phase was analyzed using an online gas chromatograph (KONIK model HRGC 4000B) equipped with a megabore column (Supel-Q PLOT, 30 m \times 0.53 mm) and a thermal conductivity detector working at a temperature of 523.15 K with helium carrier gas. The temperature of the column and the flow rate and pressure of the carrier gas were adjusted to 313.15 K, 5.0 mL \cdot min $^{-1}$, and 530 kPa, respectively. The vapor sample was taken in the sampling loop of 10 μL by a valco six-way, gas-sampling valve (GSV) the temperature of which was adjusted to 313.15 K. For the calibration of gas chromatograph, the volumetric procedure described below was used to determine the mixed gas composition, the accuracy of which was checked by the gravimetric method.

The operation of the apparatus was such that at first a known mass (about 10 g) of an ionic liquid was introduced into the equilibrium cell, and then the whole equipment (except for gas containers C1 through C3) was evacuated to pressures below 0.1 kPa by a vacuum pump and the temperature was raised to 343 K. The ionic liquid inside the cell was kept at this temperature under vacuum for at least 48 h to remove trace amounts of water and volatile impurities. The water content of ionic liquids was carefully determined before the solubility measurements by a Mettler model DL-37 Karl Fischer volumetric titrator. In all cases, the water mass fraction was found to be below $(1 \pm 0.1) \times 10^{-4}$ (Several tests were performed to check the time and the conditions for drying and degassing the ionic liquid samples. It was found that the IL was appropriately degassed and dried after pumping it under a pressure of 0.1 kPa for about 24 h at a fixed temperature of 343 K). The temperature was then adjusted to the desired value through the air bath, and a known amount of H_2S was introduced through valves V9 and CV (check valve) into the gas container C4 from the gas container C2 of known volume while valve V10 was closed. Then the whole system except for gas containers C1 through C4 was evacuated again after which a known amount of CO_2 was charged from C1 to C4 through V9 and CV. The presence of check valve CV and also the higher pressure of C1 relative to C4 (filled at first with H_2S gas) ensures that no flashback of H_2S into gas container C1 and the other parts of the system will occur during the entrance of CO_2 into the C4 container. One can calculate the total number of moles n_{gas} of H_2S and/or CO_2 injected into the equilibrium cell from

$$n_{\text{gas}} = \frac{V_{\text{gc}}}{RT_{\text{gc}}} \left(\frac{P_i}{Z_i} - \frac{P_f}{Z_f} \right) \quad (1)$$

where V_{gc} denotes the volume of the gas container (C1 or C2), Z_i and Z_f are the compressibility factors corresponding to the initial and final pressures P_i and P_f , respectively, in the gas container before and after transferring H_2S or CO_2 , and T_{gc} is the temperature of the gas container. The most accurate PVT data presented by National Institute of Standards and Technology (NIST) for pure compounds³⁴ was used to calculate compressibility factors of H_2S and CO_2 gases, which were needed for solubility calculations. In the next stage, valve

V10 was opened to allow contacting and mixing between liquid IL and vapor phases inside the equilibrium cell (EC). Equilibration, which was indicated by the constant pressure of the EC with time, was achieved normally within about 12 h by the continuous operation of a magnetic stirrer, after which valve V10 was closed. Then a few microliters of the representative equilibrated gas phase containing H_2S and CO_2 was injected from C4 through gas sampling valve GSV into the GC to analyze and determine the composition of the representative gas mixture above the gas-saturated IL. The GC analysis was performed many times for at least four repeatable outcomes, and then the average value was employed for doing the calculations. By knowing the composition of the gas phase above the IL saturated with $\text{CO}_2/\text{H}_2\text{S}$ gas mixture, together with the equilibrium total pressure, P_{equil} , the equilibrium temperature, T , and the total volume of the gas phase (which is the sum of C4 and the gas phase volume in the equilibrium cell EC), the moles of remaining H_2S and CO_2 in the gas phase, $n_{\text{gas}}^{\text{g}}$, were determined by using an appropriate equation of state and mixing rule. In this work, $n_{\text{gas}}^{\text{g}}$ was calculated using the SUPERTRAPP,³⁵ which employs the NIST extended corresponding states model (EXCST) for the calculation of phase properties. In cases where the final equilibrium pressure P_{equil} was low (below 200 kPa), the operation was altered in such a way that at first an adequate amount of helium gas was injected from C3 to the equilibrated $\text{H}_2\text{S} + \text{CO}_2$ gas mixture in C4, while valve V10 was closed, and after an additional 12 h to achieve a homogeneous composition gas mixture inside C4, the analysis of the gas mixture was performed by the above-mentioned procedure. The moles of H_2S and CO_2 in the liquid phase $n_{\text{gas}}^{\text{l}}$ were then determined from

$$n_{\text{gas}}^{\text{l}} = n_{\text{gas}} - n_{\text{gas}}^{\text{g}} \quad (2)$$

■ CORRELATION AND MODELING DETAILS

Three correlation methods were applied to the experimental data obtained in this work. The first method used was the Krichevsky–Kasarnovsky (KK) equation,³² which does not take into account the nonideality of the solute in the liquid phase

$$\ln \frac{f_i(T, P)}{x_i} = \ln K_{h, x_i}^{(P^s)}(T) + \frac{V_i^{\infty}(P - P^s)}{RT} \quad (3)$$

where $f_i(T, P)$ is the fugacity of gas solute carbon dioxide or hydrogen sulfide in the gas phase at temperature T and pressure P , x_i is the mole fraction of solute i in the solvent, $K_{h, x_i}^{(P^s)}(T)$ is Henry's law constant on mole-fraction scale of gas solute i in solvent (at vapor pressure P^s of solvent),³⁶ V_i^{∞} is the partial molar volume of gas solute i at infinite dilution, and R is the universal gas constant. In this case, the vapor pressure of the ionic liquid solvent is negligible, and it is reasonable to assume the saturated vapor pressure P^s to be zero. Equation 3 can then be rearranged to eq 4

$$\ln \frac{f_i^0(T, P)}{x_i} = \ln K_{h, x_i}^{(0)}(T) + \frac{V_i^{\infty} P}{RT} \quad (4)$$

Values of $K_{h, x_i}^{(0)}(T)$ and V_i^{∞} at each temperature T can be obtained from the intercept and slope of plots of $\ln(f_i^0/x_i)$ vs P for binary CO_2/IL or $\text{H}_2\text{S}/\text{IL}$ mixtures at the specified temperature, respectively. Here, f_i^0 is the fugacity of pure CO_2 or H_2S at equilibrated temperature T and pressure P for the gas solute/IL binary system.

The second method used was the extended Henry's law, which takes into account the nonideality of the solute, CO₂ or H₂S, in the liquid IL phase by Pitzer's activity coefficient model

$$K_{h,m_i}(T, P) a_{m_i}(T, m_i) = f_i(T, P) \quad (5)$$

$K_{h,m_i}(T, P)$ is the molality-scale Henry's law constant of the i th solute (CO₂ or H₂S) in the IL at temperature T and pressure P . $a_{m_i}(T, m_i)$ is the activity of the i th gas solute in the liquid phase (IL), which is related to the molality m_i of the gas solute and activity coefficient γ_i through eq 6:

$$a_{m_i}(T, m_i) = \frac{m_i}{m^\circ} \gamma_i \quad (6)$$

where $m^\circ = 1 \text{ mol}\cdot\text{kg}^{-1}$. The relation between $K_{h,m_i}(T, P)$ and Henry's law constant at zero pressure, $K_{h,m_i}^{(0)}(T)$, is expressed as³⁶

$$K_{h,m_i}(T, P) = K_{h,m_i}^{(0)}(T) \exp\left(\frac{V_i^\infty P}{RT}\right) \quad (7)$$

The activity coefficient of solute, γ_i , in the IL was calculated using the Pitzer's virial expansion for the excess Gibbs free energy (molality scale):^{26,27}

$$\ln \gamma_i = 2 \sum_{j=\text{CO}_2, \text{H}_2\text{S}} \frac{m_j}{m^\circ} \beta_{2i,j} + 3 \sum_{j=\text{CO}_2, \text{H}_2\text{S}} \sum_{k=\text{CO}_2, \text{H}_2\text{S}} \left(\frac{m_j}{m^\circ}\right) \left(\frac{m_k}{m^\circ}\right) \times \beta_{3i,j,k} \quad (8)$$

Here β_2 and β_3 are the parameters describing binary and ternary interactions between gas molecules in the solvent, respectively.

The fugacity of pure gas (H₂S or CO₂), $f_i^0(T, P)$, is the product of the total pressure P and fugacity coefficient $\phi_i(T, P)$ of pure gas

$$f_i^0(T, P) = \phi_i(T, P) P \quad (9)$$

Henry's law constant on the molality scale, $K_{h,m_i}^{(0)}(T)$, is related to Henry's law constant on the mole fraction scale, $K_{h,x_i}^{(0)}(T)$, by

$$K_{h,m_i}^{(0)}(T) = K_{h,x_i}^{(0)}(T) \times \frac{M_{\text{solv}}}{1000} \quad (10)$$

where M_{solv} is the relative molar mass of the solvent.

It must be added that the reason behind the selection of Pitzer's activity coefficient model for electrolytes is its simplicity and good correlative accuracy. Our previous studies^{24,25} and those made by Maurer and co-workers³⁷⁻³⁹ revealed high correlative accuracy of the Pitzer's model for gas/IL systems.

Finally the third model was the one proposed by Shiflett and Yokozeki,²⁸⁻³¹ which is a generic Redlich-Kwong (RK) type of cubic equations of state (EoS) with a simple modification to be applicable to gas-ionic liquid binary systems. The notion behind the selection of the RK EoS is the special form of the semi-theoretical mixing rule proposed by Yokozeki in his original work for the solubility of refrigerants in various lubricants.⁴⁰ Yokozeki argued that, for a binary mixture of two species with very different molecular sizes, that is, in the case of only geometrically constrained asymmetric mixtures, the assumption of random mixing of molecular species with nearly equal size is no longer valid. Then, quadratic and symmetric $x_i x_j$ terms of the second virial coefficient cannot theoretically work

as a statistical weight. Yokozeki⁴⁰ applied the random mixing concept to the highly asymmetric mixtures by rescaling the molecular sizes so that the number of neighboring interactions becomes geometrically symmetric. This is equivalent to the renormalization of the mole fraction: stretching and/or shrinking of mole fraction coordinates.⁴⁰ It must be added that each of cubic EoS's like Peng-Robinson, van der Waals, and Redlich-Kwong can be equally well-applied for performing the ϕ - ϕ calculations. In this study the RK type of EoS, as used by Shiflett and Yokozeki for gas/IL systems, was arbitrarily chosen. In this method, which is a conventional ϕ - ϕ approach, the nonideality of gas solute in the liquid IL phase as well as in the gas phase is both taken into account by the fugacity coefficient of each component calculated from the RK cubic EoS. The RK EoS is given in the following form²⁸⁻³¹

$$P = \frac{RT}{\bar{V} - b} - \frac{a(T)}{\bar{V}(\bar{V} + b)} \quad (11)$$

$$a(T) = 0.427480 \frac{R^2 T_c^2}{P_c} \alpha(T) \quad (12)$$

$$b = 0.08664 \frac{RT_c}{P_c} \quad (13)$$

where P_c and T_c are the critical pressure and critical temperature of pure components, respectively, and \bar{V} is the molar volume. The mathematical form of $\alpha(T)$ is represented by eq 14²⁸⁻³¹

$$\alpha(T) = \sum_{k=0}^{\leq 3} \lambda_k (T_r^{-1} - T_r)^k \quad (14)$$

Here $T_r = T/T_c$ is the reduced temperature, and λ_k 's are simply adjustable parameters obtained by fitting eqs 11 through 14 to experimental solubility PTx data for the systems of interest (next section).

■ COMPUTATIONAL DETAILS

Quantum chemical calculations were performed using the Gaussian version 03 package.⁴¹ The geometries were optimized at the DFT/B3LYP level of theory using the 6-311+G* and 6-311++G(2d,2p) basis sets. The calculations were carried out under isolated conditions. The binding energies, E_{binding} , calculated according to eq 15 were corrected for the basis set superposition error (BSSE)⁴² using the counterpoise method.⁴³

$$E_{\text{binding}} = E_{\text{complex}} - E_{\text{monomer1}} - E_{\text{monomer2}} \quad (15)$$

where E_{complex} and E_{monomer} stand for the counterpoise-corrected optimized energy of the supermolecule (complex) and optimized energy of each of the monomers constituting the complex, respectively. For each of the complexes, two or three initial configurations were constructed for geometry optimization to explore the potential energy surface better. Frequency calculations were carried out to verify whether the optimized structures obtained are a transition state or correspond to the most stable structure.

■ RESULTS AND DISCUSSION

Experimental Data. The data corresponding to measurement of carbon dioxide and hydrogen sulfide solubility in the ionic liquid [C₈mim][Tf₂N] at temperatures of 303.15, 313.15, 323.15, 333.15, 343.15, and 353.15 K and pressures up to about

Table 1. Mole Fraction Solubility of Carbon Dioxide Gas, x_2 , in $[\text{C}_8\text{mim}][\text{Tf}_2\text{N}]$

p/MPa	x_2	p/MPa	x_2	p/MPa	x_2
$T/K = 303.15$		$T/K = 313.15$		$T/K = 323.15$	
0.1123	0.0415 ± 0.0010	0.1193	0.0385 ± 0.0008	0.1258	0.0362 ± 0.0007
0.2488	0.0896 ± 0.0021	0.2645	0.0836 ± 0.0018	0.2793	0.0786 ± 0.0015
0.4147	0.1380 ± 0.0032	0.4405	0.1297 ± 0.0027	0.4649	0.1227 ± 0.0024
0.6362	0.2019 ± 0.0047	0.6761	0.1905 ± 0.0040	0.7138	0.1806 ± 0.0035
0.9400	0.2753 ± 0.0064	1.0001	0.2612 ± 0.0055	1.0567	0.2486 ± 0.0048
1.2389	0.3384 ± 0.0078	1.3171	0.3243 ± 0.0068	1.3932	0.3095 ± 0.0060
1.5893	0.4012 ± 0.0093	1.6922	0.3846 ± 0.0081	1.7909	0.3685 ± 0.0071
$T/K = 333.15$		$T/K = 343.15$		$T/K = 353.15$	
0.1321	0.0342 ± 0.0006	0.1381	0.0326 ± 0.0005	0.1440	0.0311 ± 0.0005
0.2934	0.0746 ± 0.0013	0.3069	0.0711 ± 0.0011	0.3196	0.0686 ± 0.0010
0.4880	0.1170 ± 0.0020	0.5101	0.1123 ± 0.0017	0.5314	0.1087 ± 0.0016
0.7501	0.1725 ± 0.0030	0.7845	0.1659 ± 0.0025	0.8176	0.1614 ± 0.0024
1.1105	0.2407 ± 0.0042	1.1616	0.2318 ± 0.0035	1.2116	0.2273 ± 0.0033
1.4650	0.2975 ± 0.0052	1.5345	0.2881 ± 0.0044	1.6008	0.2841 ± 0.0042
1.8856	0.3562 ± 0.0062	1.9760	0.3445 ± 0.0053	2.0628	0.3433 ± 0.0051

Table 2. Mole Fraction Solubility of Hydrogen Sulfide Gas, x_2 , in $[\text{C}_8\text{mim}][\text{Tf}_2\text{N}]$

p/MPa	x_2	p/MPa	x_2	p/MPa	x_2
$T/K = 303.15$		$T/K = 313.15$		$T/K = 323.15$	
0.0935	0.0807 ± 0.0010	0.1025	0.0770 ± 0.0010	0.1111	0.0719 ± 0.0008
0.2007	0.1672 ± 0.0021	0.2206	0.1599 ± 0.0022	0.2394	0.1497 ± 0.0016
0.3456	0.2744 ± 0.0035	0.3815	0.2626 ± 0.0036	0.4153	0.2472 ± 0.0027
0.5132	0.3840 ± 0.0048	0.5686	0.3674 ± 0.0050	0.6197	0.3473 ± 0.0038
0.6824	0.4753 ± 0.0060	0.7593	0.4521 ± 0.0061	0.8324	0.4309 ± 0.0047
0.8714	0.5556 ± 0.0070	0.9757	0.5317 ± 0.0072	1.0731	0.5101 ± 0.0055
1.0755	0.6222 ± 0.0079	1.2116	0.5982 ± 0.0081	1.3411	0.5756 ± 0.0062
1.3654	0.7045 ± 0.0089	1.5558	0.6673 ± 0.0091	1.7395	0.6520 ± 0.0071
1.5087	0.7355 ± 0.0093				
$T/K = 333.15$		$T/K = 343.15$		$T/K = 353.15$	
0.1191	0.0676 ± 0.0007	0.1270	0.0662 ± 0.0006	0.1343	0.0630 ± 0.0006
0.2576	0.1413 ± 0.0015	0.2748	0.1382 ± 0.0012	0.2907	0.1316 ± 0.0011
0.4473	0.2339 ± 0.0024	0.4777	0.2279 ± 0.0021	0.5062	0.2176 ± 0.0019
0.6706	0.3305 ± 0.0034	0.7175	0.3185 ± 0.0027	0.7624	0.3048 ± 0.0027
0.9012	0.4119 ± 0.0043	0.9655	0.3952 ± 0.0033	1.0270	0.3851 ± 0.0034
1.1663	0.4899 ± 0.0051	1.2539	0.4717 ± 0.0041	1.3371	0.4576 ± 0.0040
1.4635	0.5544 ± 0.0057	1.5771	0.5357 ± 0.0049	1.6869	0.5181 ± 0.0047
1.9119	0.6300 ± 0.0065				

2.0 MPa are summarized in Tables 1 and 2, respectively. As mentioned before, because of discrepancies observed between the Henry's law constants previously reported by Rahmati et al.²¹ and those obtained for other members of $\text{H}_2\text{S}/[\text{C}_n\text{mim}][\text{Tf}_2\text{N}]$, the binary system $\text{H}_2\text{S}/[\text{C}_6\text{mim}][\text{Tf}_2\text{N}]$ was again studied in this work to overcome this difficulty. The obtained PTx data for the latter system are presented in Table 3. Figures 2, 3, and 4 graphically depict the experimental data in Tables 1, 2, and 3 as Px isotherms for comparison with the correlations. The reliability and accuracy of the method of measurement have been checked in our previous works.^{20,23} Values of $K_{h,x}^{(0)}$ at each temperature T are listed in Table 4 for the solubilities of H_2S and CO_2 in the ILs studied in this work along with their standard deviations. The fugacity coefficients were calculated using SUPERTRAPP developed by NIST for pure compounds and mixtures.³⁵ The $K_{h,x}^{(0)}$ values obtained showed good correlations with temperature by the following equation

$$\ln(K_{h,x}^{(0)}/\text{MPa}) = \sum_{i=-1}^1 A_i(T/K)^i \quad (16)$$

The obtained parameters A_i of eq 16 are summarized in Table 5. The deviation between experimental and correlated Henry's law constants by means of eq 16 is within experimental uncertainties for $K_{h,x}^{(0)}$ given in Table 4. The Henry's law constants are compared with each other in Figure 5 as a function of temperature. It can be observed that the solubilities of hydrogen sulfide and carbon dioxide in $[\text{C}_8\text{mim}][\text{Tf}_2\text{N}]$ as well as in $[\text{C}_6\text{mim}][\text{Tf}_2\text{N}]$ decreases by increasing the temperature and that their solubility behavior is typical of that of physical solvents,²⁰ therefore obeying Henry's law. Also the solubility of H_2S is about two times as much as that of CO_2 in $[\text{C}_8\text{mim}][\text{Tf}_2\text{N}]$ in the entire temperature range studied in this work. We found that there exists a relatively good linear correlation between $K_{h,x}^{(0)}$ and n for dissolution of both H_2S and CO_2 in $[\text{C}_n\text{mim}][\text{Tf}_2\text{N}]$ at each temperature (especially at lower temperatures) represented by eq 17.

$$K_{h,x}^{(0)}/\text{MPa} = \delta_0 + \delta_1 n \quad (17)$$

Table 3. Mole Fraction Solubility of Hydrogen Sulfide Gas, x_2 , in $[C_6mim][Tf_2N]$

p/MPa	x_2	p/MPa	x_2	p/MPa	x_2
$T/K = 303.15$		$T/K = 313.15$		$T/K = 323.15$	
0.0685	0.0539 ± 0.0005	0.0767	0.0503 ± 0.0003	0.0846	0.0442 ± 0.0004
0.1466	0.1118 ± 0.0010	0.1637	0.1040 ± 0.0006	0.1805	0.0962 ± 0.0009
0.2276	0.1679 ± 0.0015	0.2543	0.1554 ± 0.0009	0.2804	0.1438 ± 0.0014
0.3150	0.2245 ± 0.0021	0.3532	0.2100 ± 0.0012	0.3904	0.1957 ± 0.0018
0.4863	0.3240 ± 0.0030	0.5459	0.3039 ± 0.0018	0.6039	0.2846 ± 0.0027
0.7703	0.4563 ± 0.0042	0.8737	0.4325 ± 0.0026	0.9748	0.4093 ± 0.0038
0.8705	0.4998 ± 0.0046	0.9910	0.4757 ± 0.0028	1.1091	0.4518 ± 0.0042
1.0105	0.5517 ± 0.0050	1.1549	0.5277 ± 0.0031	1.2967	0.5036 ± 0.0047
1.1789	0.6078 ± 0.0056	1.3568	0.5840 ± 0.0035	1.5317	0.5598 ± 0.0053
1.3578	0.6619 ± 0.0060	1.5740	0.6477 ± 0.0038		
1.5043	0.7012 ± 0.0064				
$T/K = 333.15$		$T/K = 343.15$		$T/K = 353.15$	
0.0924	0.0421 ± 0.0003	0.0999	0.0391 ± 0.0004	0.1073	0.0368 ± 0.0004
0.1966	0.0887 ± 0.0007	0.2123	0.0819 ± 0.0009	0.2271	0.0761 ± 0.0008
0.3056	0.1332 ± 0.0010	0.3299	0.1236 ± 0.0013	0.3532	0.1151 ± 0.0012
0.4262	0.1821 ± 0.0014	0.4609	0.1670 ± 0.0018	0.4942	0.1567 ± 0.0016
0.6605	0.2616 ± 0.0020	0.7147	0.2452 ± 0.0026	0.7668	0.2298 ± 0.0024
1.0726	0.3870 ± 0.0029	1.1665	0.3662 ± 0.0039	1.2570	0.3469 ± 0.0036
1.2235	0.4288 ± 0.0032	1.3339	0.4069 ± 0.0043	1.4391	0.3868 ± 0.0040
1.4352	0.4798 ± 0.0036	1.5683	0.4571 ± 0.0049	1.6950	0.4363 ± 0.0045
1.7012	0.5359 ± 0.0040	1.8633	0.5131 ± 0.0054	2.0168	0.4922 ± 0.0051

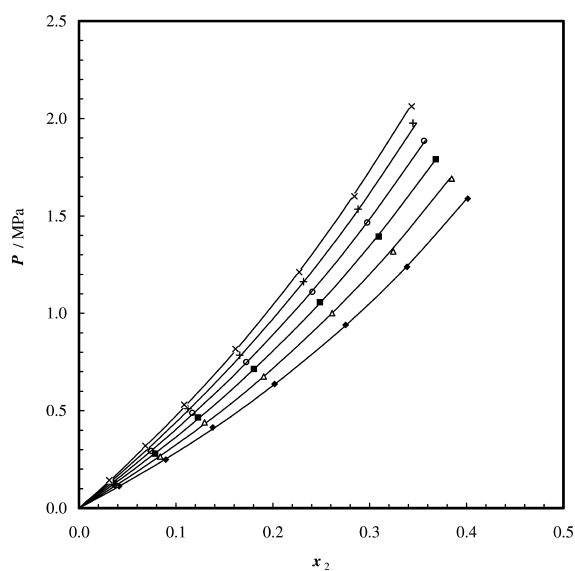


Figure 2. Total pressure above the solution of $CO_2 + [C_8mim][Tf_2N]$: \blacklozenge , 303.15 K; \triangle , 313.15 K; \blacksquare , 323.15 K; \circ , 333.15 K; $+$, 343.15 K; \times , 353.15 K; —, correlation by Pitzer's model.

The temperature variation of coefficients δ_0 and δ_1 for $H_2S/[C_nmim][Tf_2N]$ are expressed by eqs 18a and 18b and by eqs 18c and 18d for $CO_2/[C_nmim][Tf_2N]$, respectively

$$\delta_0 = \frac{-1.9853795}{(T/K)} + 0.6055446 - 0.0022733(T/K) \quad H_2S \quad (18a)$$

$$\delta_1 = \frac{1.0025309}{(T/K)} - 10.4504372 + 0.0401737(T/K) \quad H_2S \quad (18b)$$

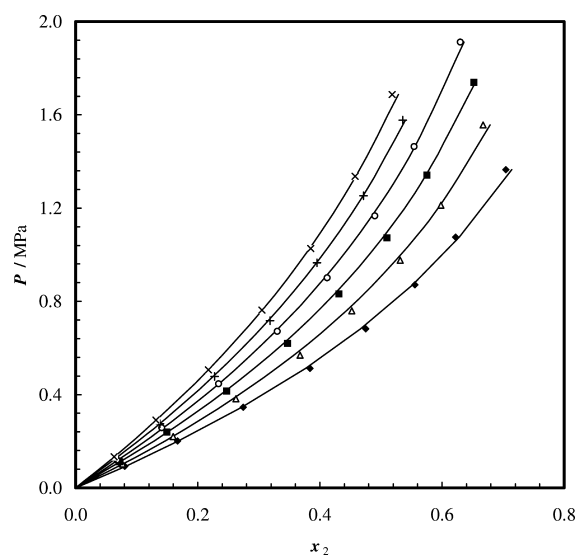


Figure 3. Total pressure above the solution of $H_2S + [C_8mim][Tf_2N]$: \blacklozenge , 303.15 K; \triangle , 313.15 K; \blacksquare , 323.15 K; \circ , 333.15 K; $+$, 343.15 K; \times , 353.15 K; —, correlation by Pitzer's model.

$$\delta_0 = \frac{0.8726564}{(T/K)} - 19.4818533 + 0.0779534(T/K) \quad CO_2 \quad (18c)$$

$$\delta_1 = \frac{1.0679905}{(T/K)} + 1.8422710 - 0.0067911(T/K) \quad CO_2 \quad (18d)$$

Equations 17 and 18 yield $K_{h,x}^{(0)}$ values as a function of temperature for solubility of H_2S and CO_2 in $[C_2mim][Tf_2N]$ through $[C_8mim][Tf_2N]$ ILs. Also Figure 5 shows that the solubilities of H_2S and CO_2 increase in $[C_nmim][Tf_2N]$ by increasing n . This same conclusion has also been made by Brennecke et al.^{8,9} for the solubility of CO_2 in classical

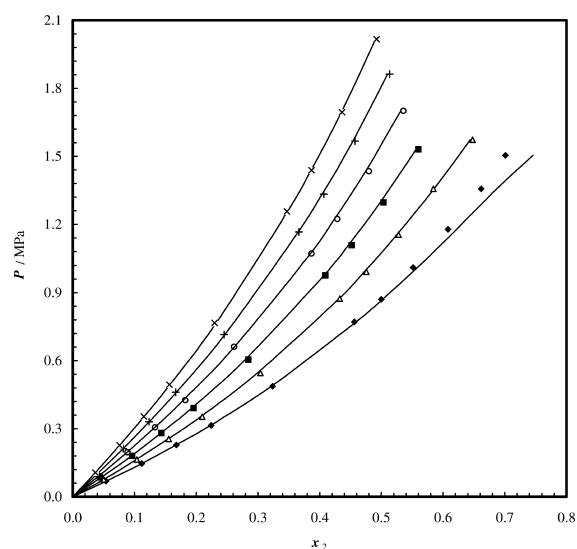


Figure 4. Total pressure above the solution of $\text{H}_2\text{S} + [\text{C}_6\text{mim}][\text{Tf}_2\text{N}]$: \blacklozenge , 303.15 K; \triangle , 313.15 K; \blacksquare , 323.15 K; \circ , 333.15 K; $+$, 343.15 K; \times , 353.15 K; —, correlation by Pitzer's model.

Table 4. Thermodynamic Properties of CO_2 and H_2S in $[\text{C}_8\text{mim}][\text{Tf}_2\text{N}]$ and $[\text{C}_6\text{mim}][\text{Tf}_2\text{N}]$

T/K	$K_{\text{h},x}^{(0)}$ (MPa)	$\Delta_{\text{sol}}G_x^\infty$ ($\text{kJ}\cdot\text{mol}^{-1}$)	$\Delta_{\text{sol}}H_x^\infty$ ($\text{kJ}\cdot\text{mol}^{-1}$)	$\Delta_{\text{sol}}S_x^\infty$ ($\text{J}\cdot\text{mol}^{-1}\cdot\text{K}^{-1}$)
$\text{CO}_2/[\text{C}_8\text{mim}][\text{Tf}_2\text{N}]$				
303.15	2.60 ± 0.04	8.22	-11.0	-63.4
313.15	2.98 ± 0.04	8.84	-10.3	-61.1
323.15	3.34 ± 0.05	9.44	-9.55	-58.8
333.15	3.71 ± 0.05	10.0	-8.79	-56.4
343.15	4.07 ± 0.06	10.6	-8.00	-54.1
353.15	4.42 ± 0.07	11.1	-7.19	-51.8
$\text{H}_2\text{S}/[\text{C}_8\text{mim}][\text{Tf}_2\text{N}]$				
303.15	0.99 ± 0.02	5.47	-13.3	-63.1
313.15	1.18 ± 0.02	5.79	-13.1	-62.5
323.15	1.36 ± 0.03	6.41	-12.7	-61.1
333.15	1.56 ± 0.03	7.01	-12.3	-59.8
343.15	1.74 ± 0.03	7.60	-11.9	-58.4
353.15	1.95 ± 0.04	8.18	-11.4	-57.1
$\text{H}_2\text{S}/[\text{C}_6\text{mim}][\text{Tf}_2\text{N}]$				
303.15	1.25 ± 0.03	6.35	-15.5	-71.9
313.15	1.51 ± 0.03	7.06	-15.2	-71.1
323.15	1.80 ± 0.04	7.77	-14.9	-70.2
333.15	2.12 ± 0.04	8.46	-14.7	-69.4
343.15	2.48 ± 0.05	9.15	-14.4	-68.6
353.15	2.86 ± 0.06	9.84	-14.1	-67.7

methylimidazolium-based ILs. To explain the observed difference in solubility, the densities of pure ILs as a function of temperature were compared to each other. A comparison reveals that the molar densities^{44,45} decrease with increasing temperature for each pure compound and their values for the ILs follow the order $[\text{C}_2\text{mim}][\text{Tf}_2\text{N}] > [\text{C}_4\text{mim}][\text{Tf}_2\text{N}] > [\text{C}_6\text{mim}][\text{Tf}_2\text{N}] > [\text{C}_8\text{mim}][\text{Tf}_2\text{N}]$. The observed trend in molar densities may be due to weaker interaction between the anion and cation,⁴⁶ which increases from $[\text{C}_2\text{mim}][\text{Tf}_2\text{N}]$ to $[\text{C}_8\text{mim}][\text{Tf}_2\text{N}]$. This effect give rise to higher free volumes in the ionic liquid, which provides an explanation from energetic and entropic point of view for the observed solubility behavior

Table 5. Numerical Values of the Parameters of Equations 16, 24, and 25a

A_{-1}	A_0	A_1	B_0 ($\text{cm}^3\cdot\text{mol}^{-1}$)	B_1 ($\text{cm}^3\cdot\text{mol}^{-1}\cdot\text{K}^{-1}$)
			$\text{CO}_2/[\text{C}_8\text{mim}][\text{Tf}_2\text{N}]$	
-2609.79	13.05286	-0.013971	1.017319	-0.231635
			$\text{H}_2\text{S}/[\text{C}_8\text{mim}][\text{Tf}_2\text{N}]$	
-2312.41	9.322106	-0.008083	-14.25479	-3.834807
			$\text{H}_2\text{S}/[\text{C}_6\text{mim}][\text{Tf}_2\text{N}]^a$	
-2358.34	8.705225	-0.00505	-154.181	-1.24214

^aFor $\beta_{2,\text{H}_2\text{S}-\text{H}_2\text{S}}$ $C_0 = 0.313928$, and $C_1 = -110.588$.

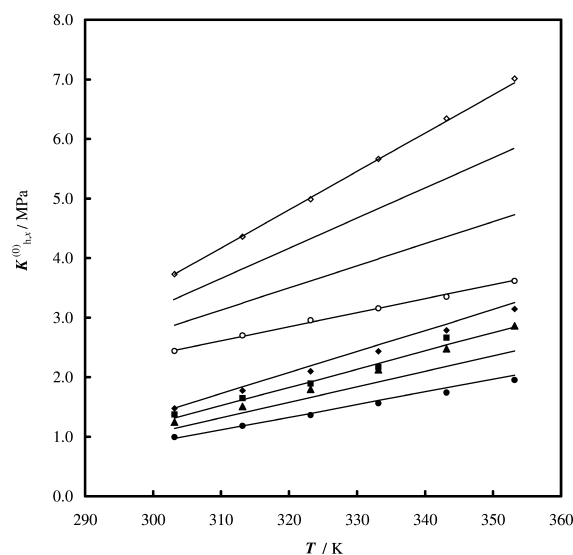


Figure 5. Comparison between Henry's law constants as a function of temperature for the solubility of H_2S and CO_2 in $[\text{C}_n\text{mim}][\text{Tf}_2\text{N}]$ ILs: \bullet , $\text{H}_2\text{S} + [\text{C}_8\text{mim}]$ (this work); \blacktriangle , $\text{H}_2\text{S} + [\text{C}_6\text{mim}]$ (this work); \blacksquare , $\text{H}_2\text{S} + [\text{C}_4\text{mim}]$ (ref 20); \blacklozenge , $\text{H}_2\text{S} + [\text{C}_2\text{mim}]$ (ref 25); \circ , $\text{CO}_2 + [\text{C}_8\text{mim}]$ (this work); \diamond , $\text{CO}_2 + [\text{C}_2\text{mim}]$ (ref 62).

of H_2S as well as CO_2 in $[\text{C}_n\text{mim}][\text{Tf}_2\text{N}]$ ILs. As the molar density of the solvent IL increases, the void (or free) volume of the IL decreases. This phenomenon causes less free space to be accessible to the H_2S or CO_2 gas solute molecules, and therefore the solubility increases from $[\text{C}_2\text{mim}][\text{Tf}_2\text{N}]$ to $[\text{C}_8\text{mim}][\text{Tf}_2\text{N}]$. Brennecke and co-workers have pointed out this same conclusion in their earlier experimental studies on the high-pressure phase behavior of IL/ CO_2 systems.^{8,47} Also Noble and co-workers⁴⁸ through the use of regular solution theory^{49,50} derived a simplified linear relation between the natural logarithm of the Henry's law constant for the solubility of CO_2 in imidazolium based ILs and the inverse of a rational power of molar volume (V_m) of the ILs, that is, $\ln(K_h^{(0)}/\text{atm}) = \chi + \kappa V_m^{-4/3}$. Their derived relation confirms the above discussions.

It can be shown that the Gibbs energy of solution, corresponding to the change in Gibbs energy when the solute is transferred at a constant temperature from the pure perfect

gas at the standard pressure to the standard state of infinite dilution of the solute in the solvent, is given by⁵¹

$$\Delta_{\text{sol}}G_x^\infty = RT \ln \left(\frac{K_{h,x}^{(0)}}{P^0} \right) \quad (19)$$

where P^0 is the standard state pressure. The partial molar differences in enthalpy and entropy between the two states can be obtained by calculating the corresponding partial derivatives of the Gibbs energy with respect to temperature

$$\Delta_{\text{sol}}H_x^\infty = -T^2 \frac{\partial}{\partial T} \left(\frac{\Delta_{\text{sol}}G_x^\infty}{T} \right) = -RT^2 \frac{\partial}{\partial T} \left[\ln \left(\frac{K_{h,x}^{(0)}}{P^0} \right) \right] \quad (20)$$

$$\Delta_{\text{sol}}S_x^\infty = \frac{(\Delta_{\text{sol}}H_x^\infty - \Delta_{\text{sol}}G_x^\infty)}{T} \quad (21)$$

The pressure range considered in this work is not high enough to cause Henry's law constant to be a strong function of pressure.^{20,21} Therefore, one would not expect large errors if one ignores this pressure dependency. By means of this approximation and using eqs 19, 20, and 21, we estimated the mole-fraction scale thermodynamic functions of solution at infinite dilution for CO₂ and H₂S in [C₆mim][Tf₂N] and [C₈mim][Tf₂N]. It may be worth mentioning that the relation between mole fraction scale and molality scale thermodynamic functions of solution is straightforward and they can be transformed to each other by using eqs 22 and 23,³⁷

$$\Delta_{\text{sol}}G_m^\infty = \Delta_{\text{sol}}G_x^\infty + RT \ln(M_{\text{solvr}}/1000) \quad (22)$$

$$\Delta_{\text{sol}}S_m^\infty = \Delta_{\text{sol}}S_x^\infty - R \ln(M_{\text{solvr}}/1000) \quad (23)$$

The values for the mole fraction scale Gibbs free energy, $\Delta_{\text{sol}}G_x^\infty$, enthalpy, $\Delta_{\text{sol}}H_x^\infty$, and entropy $\Delta_{\text{sol}}S_x^\infty$ of solution are given in Table 4 at temperatures from 303.15 to 353.15 K for CO₂/[C₈mim][Tf₂N], H₂S/[C₈mim][Tf₂N], and H₂S/[C₆mim][Tf₂N], respectively. As it can be observed, the $\Delta_{\text{sol}}G_x^\infty$ values are positive and increase with temperature in a similar manner for the three systems, being the highest for CO₂/[C₈mim][Tf₂N] and the lowest for H₂S/[C₆mim][Tf₂N]. The $\Delta_{\text{sol}}H_x^\infty$ values are negative, and the variations with temperature of the $\Delta_{\text{sol}}H_x^\infty$ values are positive for CO₂/[C₈mim][Tf₂N], H₂S/[C₈mim][Tf₂N], and H₂S/[C₆mim][Tf₂N] binary mixtures; that is, they increase with temperature. The interaction of CO₂ with ILs includes dispersion, dipole-induced dipole, and electrostatic forces. In addition to the above interactions, H₂S also exhibits hydrogen bonding with the anion part of the ILs.¹⁷ The $\Delta_{\text{sol}}H_x^\infty$ values of CO₂ and H₂S dissolution in [C₈mim][Tf₂N] and [C₆mim][Tf₂N] are similar to those of polar solvents such as water, methanol, and ethanol, which physically absorb these gases, where the interactions are dispersion and dipole-induced dipole, but not electrostatic. The $\Delta_{\text{sol}}H_x^\infty$ values for CO₂ and H₂S absorption into nonpolar solvents such as cyclohexane and heptane tend to be smaller due to limited dispersion forces.⁴⁷ Heat of absorption values for compounds affording chemical reaction and complexation, such as alkanolamines, are much larger.² We have also compared the $\Delta_{\text{sol}}H_x^\infty$ values for the dissolution of CO₂ and H₂S in some ILs in Figure 6. Generally, it can be deduced that the absorption of H₂S in ILs is more energetic than that of CO₂ indicating that

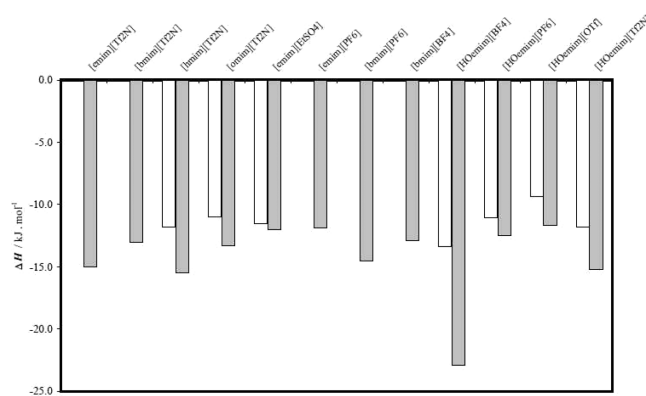


Figure 6. Comparison of the partial molar heats of absorption at infinite dilution, $\Delta_{\text{sol}}H_x^\infty$, for CO₂ and H₂S in ionic liquids: gray columns, H₂S; white columns, CO₂.

the interaction of H₂S with the cation and anion of the ILs is stronger than that of CO₂. This is also confirmed in the next section, where the ab initio quantum chemical calculations yield this same conclusion in the case of interaction energy of H₂S and CO₂ with [C_nmim][Tf₂N]. In addition, it can be observed from Figure 6 that the $\Delta_{\text{sol}}H_x^\infty$ values for the dissolution of pure CO₂ in the ILs are comparable with each other and except for 1-(2-hydroxyethyl)imidazolium tetrafluoroborate ([HOemim]-[BF₄]), there is no significant difference between their values. This same behavior can be observed for dissolution of H₂S in the ILs. The comparison between the $\Delta_{\text{sol}}H_x^\infty$ values reveals that the interaction of H₂S is more energetic than CO₂ with [C₈mim][Tf₂N]. Also, the interaction of H₂S is more energetic with [C₆mim][Tf₂N] than with [C₈mim][Tf₂N]. The $\Delta_{\text{sol}}S_x^\infty$ values show the degree of ordering in the solution associated with the gas dissolution. It can be seen from Table 4 that more ordering occurs with H₂S than does with CO₂ in the [C₆mim][Tf₂N] and [C₈mim][Tf₂N] ionic liquids, but the difference is not so high to carry out further analysis indicating that the energetic effect is more important than the entropic effect. Table 4 reveals that, as in the case of $\Delta_{\text{sol}}H_x^\infty$, the $\Delta_{\text{sol}}S_x^\infty$ values are negative and the variation with temperature of the $\Delta_{\text{sol}}S_x^\infty$ values are positive for CO₂/[C₈mim][Tf₂N], H₂S/[C₈mim][Tf₂N], and H₂S/[C₆mim][Tf₂N] binary mixtures; that is, they increase with temperature.

The H₂S/CO₂/[C₈mim][Tf₂N] ternary system was also studied to assess the feasibility of the H₂S/CO₂ gas separation by the selective absorption method. The solubility experiments were performed under various T , P , and feed compositions. Three levels were selected for the molar ratios of hydrogen sulfide to carbon dioxide in the feed, that is, H₂S/CO₂ \approx 4:1, 1:1, and 1:4. Special care was taken when preparing the H₂S/CO₂ gas mixtures to prevent the H₂S from condensing. The saturation vapor pressure for H₂S at 298 K (2.0173 MPa) is lower than that of CO₂ at 298 K (6.4342 MPa). Therefore, the total pressure for the three feed gas mixtures was set below 2.0 MPa. All measurements were carried out at temperatures of 303.15, 323.15, and 343.15 K and pressures less than 1.3 MPa. The experimental results for the H₂S/CO₂/[C₈mim][Tf₂N] ternary system are summarized in Table 6. Discussions about modeling and gas separation feasibility are presented in the next section.

Results of Correlation of Experimental Data. As mentioned in previous section, the Pitzer's and RK models were used to correlate the experimental solubility data. In case

Table 6. Experimental VLE Data for CO₂/H₂S/[C₈mim][Tf₂N] Ternary Mixtures

feed ^a				measured			calculated			
CO ₂	H ₂ S	IL	T/K	P/MPa	100·x _{H₂S}	100·x _{IL}	100·y _{H₂S}	100·x _{H₂S}	100·x _{IL}	100·y _{H₂S}
5.1	20.1	74.8	303.15	0.1717	12.0	86.5	72.2	12.3	86.2	71.5
9.1	34.4	56.5	303.15	0.3821	24.0	73.2	70.0	24.4	72.7	69.4
12.5	49.8	37.7	303.15	0.7678	40.0	55.2	70.8	40.9	54.9	69.3
13.6	14.7	71.7	303.15	0.2275	9.0	86.6	42.1	9.4	86.3	40.9
22.1	23.7	54.2	303.15	0.4750	17.0	74.8	41.3	17.9	74.3	39.5
27.3	30.0	42.7	303.15	0.7214	24.6	64.1	40.8	25.3	64.4	39.3
19.2	4.8	76.0	303.15	0.2051	2.9	91.0	14.0	3.0	90.7	14.1
35.3	9.2	55.5	303.15	0.5005	6.8	79.1	14.8	7.0	79.2	14.3
48.6	12.1	39.3	303.15	0.9603	11.4	66.8	13.1	11.6	66.0	12.9
5.0	20.1	74.9	323.15	0.2039	10.5	88.2	74.8	10.7	88.1	74.1
9.0	35.1	55.9	323.15	0.4600	22.1	75.2	72.9	21.8	75.7	72.5
12.6	50.4	37.0	323.15	0.9249	38.5	57.0	72.3	37.4	58.7	72.4
13.8	14.6	71.6	323.15	0.2639	8.1	88.1	42.6	8.0	88.2	42.9
22.4	23.4	54.2	323.15	0.5496	15.5	77.2	41.9	15.5	77.5	41.7
26.9	29.0	44.1	323.15	0.8443	21.7	68.0	42.7	22.3	68.2	41.3
19.2	4.9	75.9	323.15	0.2325	2.6	91.9	15.7	2.6	92.0	15.6
35.2	8.9	55.9	323.15	0.5677	6.0	81.8	15.4	6.0	81.9	15.2
48.6	12.3	39.1	323.15	1.0900	10.3	69.2	14.9	10.5	69.5	14.6
4.8	19.7	75.5	343.15	0.2237	9.3	89.5	75.4	8.9	90.1	75.7
8.5	35.5	56.0	343.15	0.5330	19.8	77.8	75.9	19.6	78.3	75.4
12.5	49.9	37.6	343.15	1.0706	34.4	61.4	74.4	33.9	62.6	74.1
13.7	14.6	71.7	343.15	0.2972	7.2	89.3	44.7	7.0	89.7	44.9
22.0	23.7	54.3	343.15	0.6201	14.4	79.3	44.1	13.9	80.0	44.6
27.2	29.6	43.2	343.15	0.9592	19.4	71.1	45.4	20.2	71.3	44.2
19.1	4.7	76.2	343.15	0.2572	2.2	93.1	15.7	2.2	93.1	16.0
34.9	9.2	55.9	343.15	0.6297	5.6	83.5	16.3	5.4	84.1	16.6
47.9	12.6	39.5	343.15	1.2077	9.5	72.5	16.4	9.6	72.6	16.3

^aConcentration units in mole %.

of Pitzer's model, the partial molar volume of gas solute *i* at infinite dilution, V_i^∞ , was considered a linear function of absolute temperature *T* defined by eq 24

$$V_i^\infty(T) = B_0 + B_1T \quad (24)$$

where V_i^∞ is in cm³·mol⁻¹ and *T* is in K. Parameters β_2 and β_3 were considered as a function of temperature *T*, defined by eqs 25a and 25b, respectively. Binary ($\beta_{2,\text{CO}_2-\text{CO}_2}$ and $\beta_{2,\text{H}_2\text{S}-\text{H}_2\text{S}}$) as well as ternary ($\beta_{3,\text{CO}_2-\text{CO}_2-\text{CO}_2}$ and $\beta_{3,\text{H}_2\text{S}-\text{H}_2\text{S}-\text{H}_2\text{S}}$) interactions in [C₈mim][Tf₂N] were described by eq 25a, and the other binary and ternary interactions (for example $\beta_{2,\text{CO}_2-\text{H}_2\text{S}}$, $\beta_{3,\text{CO}_2-\text{H}_2\text{S}-\text{H}_2\text{S}}$, etc.) were described by eq 25b. Neglect of the parameter β_3 does not have a considerable effect on the accuracy of correlation for any of H₂S/IL and CO₂/IL binary mixtures, but they need to be considered for improving the accuracy of correlation for ternary H₂S/CO₂/[C₈mim][Tf₂N] mixtures. Also for H₂S/CO₂/[C₈mim][Tf₂N] ternary mixtures the binary interaction parameters $\beta_{2,\text{CO}_2-\text{H}_2\text{S}}$ and $\beta_{2,\text{H}_2\text{S}-\text{CO}_2}$ were considered different, that is, $\beta_{2,\text{CO}_2-\text{H}_2\text{S}} \neq \beta_{2,\text{H}_2\text{S}-\text{CO}_2}$, to improve the correlation accuracy of the Pitzer's model, while in the case of binary gas/IL mixtures they were considered equal.

$$X = C_0 + \frac{C_1}{T/K} \quad (i = j = k) \quad (25a)$$

$$X = D_0 + D_1(T/K) \quad (\text{other cases}) \quad (25b)$$

where $X = \beta_{2ij}$ and β_{3ijk} . The obtained parameters B_0 and B_1 of eq 24 are summarized in Table 5; the fitted parameters C_0 , C_1 ,

D_0 , and D_1 of eqs 25 for CO₂/[C₈mim][Tf₂N], H₂S/[C₈mim][Tf₂N], and H₂S/CO₂/[C₈mim][Tf₂N] systems are presented in Table 7, and the parameters C_0 and C_1 for H₂S/

Table 7. Numerical Values of the Parameters of Equations 25a and 25b for Binary and Ternary Interactions of CO₂, H₂S, and Their Mixture in [C₈mim][Tf₂N]

interaction	β_2 or β_3	
CO ₂ -CO ₂	$C_0 = -0.054653$	$C_1 = 3.907633$
H ₂ S-H ₂ S	$C_0 = 0.746299$	$C_1 = -226.762$
CO ₂ -H ₂ S	$D_0 = 2.22527$	$D_1 = -0.012500$
H ₂ S-CO ₂	$D_0 = 0.206944$	$D_1 = -0.009390$
CO ₂ -CO ₂ -CO ₂	$C_0 = -0.005110$	$C_1 = 1.52465$
H ₂ S-H ₂ S-H ₂ S	$C_0 = -0.004750$	$C_1 = 1.542520$
H ₂ S-CO ₂ -H ₂ S	$D_0 = -1.61504$	$D_1 = 0.006799$
CO ₂ -H ₂ S-CO ₂		

[C₆mim][Tf₂N] are presented at the footnote of Table 5. The correlations made by the Pitzer's model for mole fraction of CO₂ and H₂S gas solutes, dissolved in the solvent IL at the specified temperature and pressure, are graphically shown in Figures 2, 3 and 4 for the three binary systems investigated in this study. It can be seen that there is quite good agreement between the correlated results and the observed experimental data in Tables 1, 2, and 3. Only in the case of the H₂S/[C₈mim][Tf₂N] binary system (Figure 4) at low temperature of 303.15 K and pressures of above 1 MPa does the Pitzer's model show relatively high positive deviations up to about 6.3%

Table 8. Pure Component Constants Used for the RK EoS^a

compound	molar mass (g·mol ⁻¹)	T _c /K	P _c /kPa	λ ₀	λ ₁	λ ₂	λ ₃
CO ₂	44.010	304.13	7377	1.00049	0.43866	-0.10498	0.06250
H ₂ S	34.082	373.10	9000	0.99879	0.33206	-0.049417	0.0046387
[C ₈ mim][Tf ₂ N]	475.48	1311.7	2096	1	0.02012	0	0
[C ₆ mim][Tf ₂ N]	447.43	1287.3	2390	1	0.05220	0	0

^aThe critical parameters for [C₆mim][Tf₂N] and [C₈mim][Tf₂N] were estimated with the method proposed by Valderrama et al.^{53,54}

in mole fraction from the experimental data. We currently do not have a reasonable explanation for this behavior.

In the case of RK model, we need the critical properties of pure compounds, extracted from NIST database for the pure compounds CO₂ and H₂S,³⁴ and for the ionic liquids [C₆mim][Tf₂N] and [C₈mim][Tf₂N], they were estimated by the modified Lydersen–Joback–Reid method,⁵² proposed by Valderrama and co-workers.^{53,54} The parameters λ₀ through λ₃ for CO₂ and H₂S were taken from ref 19, which were obtained by Shiflett and Yokozeki from the corresponding vapor pressure data, and those of the IL were obtained through analysis of *PTx* solubility data for each of the three systems investigated in this work. The parameters λ₀ through λ₃ together with the critical constants are presented in Table 8 for each pure compound. The parameters *a* and *b* (eqs 12 and 13) were modeled by the modified van der Waals–Berthelot mixing rule proposed by Yokozeki⁴⁰ for general *N*-component mixtures as follows

$$a(T) = \sum_{i,j=1}^N \sqrt{a_i a_j} f_{ij}(T) (1 - k_{ij}) x_i x_j \quad (26)$$

$$b = \frac{1}{2} \sum_{i,j=1}^N (b_i + b_j) (1 - m_{ij}) (1 - k_{ij}) x_i x_j \quad (27)$$

$$f_{ij}(T) = 1 + \frac{\tau_{ij}}{T} \quad (28)$$

$$k_{ij} = \frac{l_{ij} l_{ji} (x_i + x_j)}{l_{ji} x_i + l_{ij} x_j} \quad (29)$$

where τ_{ij} = τ_{ji}, τ_{ii} = 0, m_{ij} = m_{ji}, m_{ii} = 0, and k_{ii} = 0. The parameters *a_i* and *b_i* are defined similar to eqs 12 and 13

$$a_i(T) = 0.427480 \frac{R^2 T_{ci}^2}{P_{ci}} \alpha_i(T) \quad (30)$$

$$b_i = 0.08664 \frac{R T_{ci}}{P_{ci}} \quad (31)$$

There are four binary interaction parameters in this model: *l_{ij}*, *l_{ji}*, *m_{ij}* and τ_{ij}, which were obtained for each binary pair using nonlinear regression analyses of experimental *PTx* data for CO₂/[C₈mim][Tf₂N], H₂S/[C₈mim][Tf₂N], and H₂S/[C₆mim][Tf₂N] binary systems. The numerical values of binary interaction parameters are summarized in Table 9. The expression for fugacity coefficient φ_{*i*} of the *i*th species for the RK EoS, which is needed for the phase equilibrium calculation, is given in refs 28 through 31. The equilibrium solubility for the

Table 9. Binary Interaction Parameters of the RK EoS^a

system 1/2	l ₁₂	l ₂₁	m ₁₂ = m ₂₁	τ ₁₂ = τ ₂₁ /K
CO ₂ /[C ₈ mim][Tf ₂ N]	0.42943	0.31444	-0.32448	23.095
H ₂ S/[C ₈ mim][Tf ₂ N]	0.21347	0.07944	-0.03478	35.000
H ₂ S/[C ₆ mim][Tf ₂ N]	0.15623	0.13236	-0.12372	51.798

^aDetermined by nonlinear least-squares analysis using the solubility data of this study.

binary and ternary systems of IL + CO₂ + H₂S can be obtained by applying the fundamental criterion for phase equilibrium:

$$x_i \hat{\phi}_i^L = y_i \hat{\phi}_i^V \quad (i = 1, 2, 3) \quad (32)$$

where *x_i* and *y_i* are liquid and vapor mole fractions of the *i*th species, and φ_{*i*}^L and φ_{*i*}^V stand for the fugacity coefficient of the *i*th species in the liquid and vapor phases, respectively.

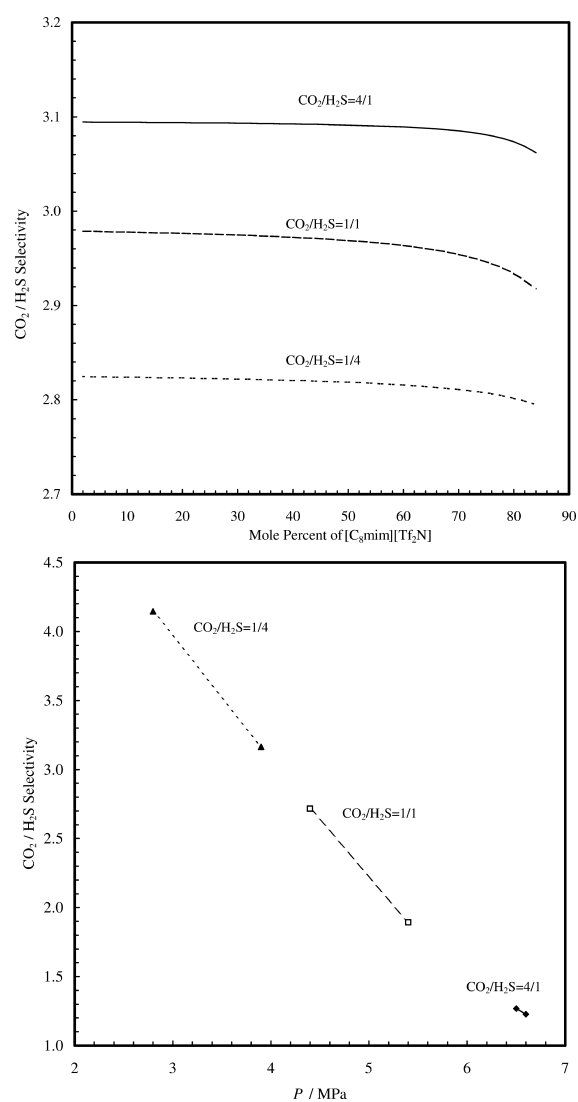
The average of relative deviations, ARD%, defined by eq 33 together with the maximum of relative deviations (MRD%) of correlated mole fractions by using each of the three models, *x_i^{cor}*, from experimental data, *x_i^{exp}*, are summarized and compared with each other in Table 10 for a number of *N* data points.

$$\text{ARD}\% = \frac{100}{N} \sum_{i=1}^N \left| \frac{x_i^{\text{cor}} - x_i^{\text{exp}}}{x_i^{\text{exp}}} \right| \quad (33)$$

Table 10 shows that the Pitzer's model correlates the solubility data of CO₂ and H₂S in [C₈mim][Tf₂N] with a higher accuracy than the RK EoS and the KK equation. In the case of CO₂, the KK equation shows a higher correlation accuracy than RK EoS, but in the case of H₂S, the RK EoS shows a higher correlation accuracy than the KK equation. In the case of CO₂/[C₈mim][Tf₂N], the solubility is lower compared to H₂S, and thus the nonideality in the liquid phase is negligible. Hence, the KK approach seems to be able to adequately describe the observed solubility behavior. In the case of H₂S/[C₆mim][Tf₂N] binary system, the RK EoS shows the highest correlation accuracy, while the Pitzer's model and KK equation have comparable accuracy with each other. In the case of the CO₂/H₂S/[C₈mim][Tf₂N] ternary system, the RK EoS shows the highest correlation accuracy. The KK equation did not employ to correlate the experimental data of the CO₂/H₂S/[C₈mim][Tf₂N] ternary system. It must be noted here that the values of the critical constants, *T_c* and *P_c*, of the ILs estimated by different methods have a negligible effect on the correlation accuracy of the RK EoS. For example in the case of [C₈mim][Tf₂N] the values of *T_c* and *P_c* change respectively from 1311.9 K and 2.10 MPa using the method of Valderrama et al.⁵³ (method I) to 1088.7 K and 1.77 MPa by using the group contribution method due to Shen et al.⁵⁵ (method II). In this case the values of ARD% change from 3.1% by using method I to 3.2% when method II is employed for the

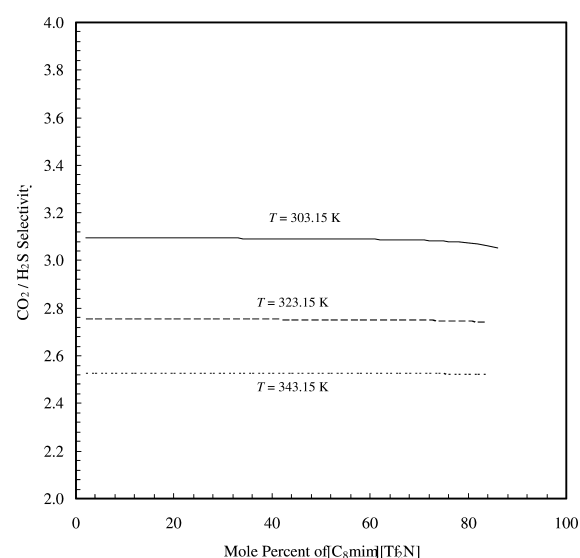
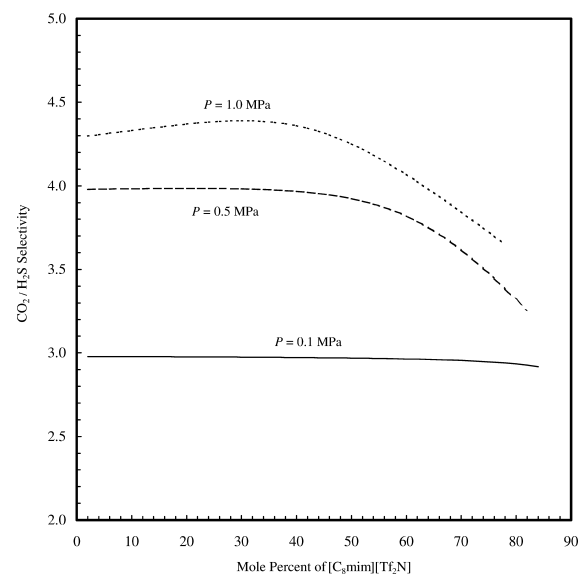
Table 10. Comparison between Average Relative Deviations (ARD %) and Maximum Relative Deviations (MRD %) Calculated from Experimental Mole Fractions by the Three Models Considered in This Work

system	Pitzer's model		KK equation		RK equation	
	ARD%	MRD%	ARD%	MRD%	ARD%	MRD%
CO ₂ /[C ₈ mim][Tf ₂ N]	0.76	3.2	0.72	2.4	3.1	7.9
H ₂ S/[C ₈ mim][Tf ₂ N]	1.0	2.8	3.3	9.9	1.7	6.9
CO ₂ /H ₂ S/[C ₈ mim][Tf ₂ N]	8.9	37			3.9	9.9
H ₂ S/[C ₆ mim][Tf ₂ N]	0.92	6.3	1.1	5.1	0.52	4.5
overall	2.9		1.7		2.3	

**Figure 7.** (a) Calculated selectivity defined by eq 34 versus [C₈mim][Tf₂N] mole percent with three different CO₂/H₂S mole ratios at $T = 303.15$ K and $P = 0.1$ MPa. (b) Selectivity plots without ionic liquid [C₈mim][Tf₂N] as a function of total pressure. Continuous line (—), 4:1 CO₂/H₂S feed mole ratio; broken line (- - -), 1:1 CO₂/H₂S feed mole ratio; dotted line (···), 1:4 CO₂/H₂S feed mole ratio.

CO₂/[C₈mim][Tf₂N] binary system, and they change from 1.77% by using method I to 1.80% using method II for H₂S/[C₈mim][Tf₂N] binary system. This is also the case for the H₂S/[C₆mim][Tf₂N] binary system. The ARD% changes from 0.37% by using method I to 0.46% when method II is used.

As mentioned before, the CO₂/H₂S/[C₈mim][Tf₂N] ternary system was also studied to investigate the possibility of gas

**Figure 8.** Plot of calculated selectivity defined by eq 34 versus [C₈mim][Tf₂N] mole percent at $T = 303.15$, 323.15 , and 343.15 K, $P = 0.1$ MPa, and CO₂/H₂S = 1:4 feed ratio. Continuous line (—), $T = 303.15$ K; broken line (- - -), $T = 323.15$ K; dotted line (···), $T = 343.15$ K.**Figure 9.** Plot of calculated selectivity defined by eq 34 versus [C₈mim][Tf₂N] mole percent at $T = 303.15$ K, $P = 0.1$ to 1.0 MPa, and CO₂/H₂S = 1:4 feed ratio. Continuous line (—), $P = 0.1$ MPa; broken line (- - -), $P = 0.5$ MPa; dotted line (···), $P = 1.0$ MPa.

separation by the absorptive method using [C₈mim][Tf₂N] ionic liquid. To do this, the RK EoS, a method experimentally proven to be accurate in the present work (see Table 10) was

used to calculate the gaseous selectivity $\alpha_{A/B}$, which is the ability to separate gases A and B in the gas phase or gaseous absorption selectivity $S_{A/B}$ in the liquid phase. These factors are defined as follows^{19,56,57}

$$\alpha_{A/B} = S_{B/A} = \frac{y_A/x_A}{y_B/x_B} \quad (34)$$

Here we denote CO₂ as A and H₂S as B; the CO₂/H₂S selectivity in the gas phase ($\alpha_{A/B}$) has been computed according to present EoS model at $T = 303.15, 323.15, \text{ and } 343.15 \text{ K}$, and the results are summarized in Figures 7 through 9. In Figure 7a, the CO₂/H₂S selectivity ($\alpha_{A/B}$) is plotted as a function of the [C₈mim][Tf₂N] mole percent for three ternary mixtures with mole ratios 4:1, 1:1, and 1:4 at $T = 303.15 \text{ K}$ and $P = 0.1 \text{ MPa}$. In all three cases, $\alpha_{A/B}$ remains relatively constant with increasing ionic liquid concentration except at high IL concentrations, in which they decrease steeply. Also it can be observed that $\alpha_{A/B}$ decreases from about 3.1 to about 2.8 as the CO₂/H₂S mole ratio decreases from 4:1 to 1:4. To understand the change in selectivity due to ionic liquid addition, Figure 7b provides clear insights, where the selectivity with no [C₈mim][Tf₂N] at 303.15 K is plotted as a function of pressure for the same CO₂/H₂S ratios (4:1, 1:1, and 1:4) in the absence of [C₈mim][Tf₂N]. The selectivity enhancement due to the ionic liquid addition can be well-observed from the comparison of Figure 7a and b. For example, the CO₂/H₂S feed ratio of 4:1 has a selectivity of about 2.8 with the ionic liquid, while the corresponding case shows a selectivity of about 1.2 without the ionic liquid (approximately the same as the value reported by Shiflett and Yokozeki¹⁹ at 298.15 K). As the CO₂/H₂S feed ratio decreases from 4:1 to 1:1 to 1:4, the improvement in selectivity with the ionic liquid versus no ionic liquid also decreases. The selectivity characteristics at higher temperatures and pressures are shown in Figures 8 and 9, respectively. It can be observed from Figure 8 that the selectivity ($\alpha_{A/B}$) decreases by increasing temperature. This behavior exists at all CO₂/H₂S feed ratios and all pressures from 0.1 to 1.0 MPa. Figure 9 shows that the selectivity increases by increasing pressure. This trend can be observed for all CO₂/H₂S feed ratios. Figure 9 also shows that the selectivity enhancement is pronounced by about 43% in going from $P = 0.1 \text{ MPa}$ to $P = 1.0 \text{ MPa}$. The most important fact to consider at higher temperatures (343.15 K) is

that, at high CO₂/H₂S feed ratios (1:1 and 4:1) without the ionic liquid, no vapor–liquid equilibria exists¹⁹ and the gas separation cannot be accomplished using traditional distillation methods. Therefore, only with the addition of the ionic liquid is the separation of CO₂ and H₂S possible.

■ COMPUTATIONAL RESULTS

In this section, discussions are presented from the molecular point of view based on gas phase quantum chemical calculations using geometrical optimizations to understand the observed trends in the experimental data measured in this article and previous related reports. As mentioned before, there is an inverse relation between the molar density of [C_{*n*}mim][Tf₂N] ionic liquids and solubility of both CO₂ and H₂S in these ILs. Thus, the intermolecular interaction energy between the isolated anion and cation of [C_{*n*}mim][Tf₂N] complexes as well as the interaction energy between CO₂ and H₂S molecules with the anion and cation counterparts of the ionic liquids were calculated to obtain an explanation for the observed experimental results. The counter-poise corrected energies of [C_{*n*}mim][Tf₂N] complexes were calculated using both the B3LYP/6-311++G(2d,2p) and B3LYP/6-311+G(d) levels to compare the trends obtained from each of the two basis sets and assess the basis set, which yields a proper description for the molecular behavior of these systems. Results of computation of molecular energies of single species, together with the interaction energies, E_{binding} for each complex, are summarized in Table 11. Figure 10 shows the geometry of the minimum energy structures obtained at the B3LYP/6-311++G(2d,2p) level of theory for the monomers and complexes studied in this work. In all [C_{*n*}mim][Tf₂N] complexes, the two sulfur atoms together with the central nitrogen atom of the [Tf₂N][−] anion are approximately coplanar with the imidazolium ring of the [C_{*n*}mim]⁺ cation. The C₂–H hydrogen in the cation (the hydrogen attached to the carbon between the two nitrogen atoms) is directed toward the nitrogen atom of the anion. The distance between C₂–H hydrogen of the cation, and the nitrogen atom of the anion does not vary considerably from [C₂mim][Tf₂N] to [C₈mim][Tf₂N] and is relatively constant in the small range of 2.017–2.027 Å, indicating that the size of the alkyl chain substituent of imidazolium ring has no considerable effect on the minimum distance between anion and cation and only affects the interaction energy between the

Table 11. Energetic and Geometric Data on [C_{*n*}mim][Tf₂N], H₂S–[Tf₂N][−] and CO₂–[Tf₂N][−] Complexes

complex	B3LYP/basis set	$E_0 + \text{ZPE}$	$E_{\text{binding}} \text{ kJ}\cdot\text{mol}^{-1}$	minimum distance	OCO or H ₂ S angle
[C ₂ mim][Tf ₂ N]	6-311+G(d)	−2172.34931565	−309.8	1.965	
	6-311++G(2d,2p)	−2172.46602623	−308.6	2.017	
[C ₄ mim][Tf ₂ N]	6-311+G(d)	−2250.99393366	−306.6	1.972	
	6-311++G(2d,2p)	−2251.11740413	−301.2	2.022	
[C ₆ mim][Tf ₂ N]	6-311+G(d)	−2329.63818784	−306.0	1.991	
	6-311++G(2d,2p)	−2329.76969237	−299.9	2.027	
[C ₈ mim][Tf ₂ N]	6-311+G(d)	−2408.28243558	−306.5	1.989	
	6-311++G(2d,2p)	−2408.42119862	−297.7	2.019	
H ₂ S–[Tf ₂ N] [−]	6-311+G(d)	−2227.03107444	−19.26	2.269	91.83
	6-311++G(2d,2p)	−2227.13641814	−31.17	2.323	91.13
CO ₂ –[Tf ₂ N] [−]	6-311+G(d)	−2016.26154895	−11.06	2.971	176.3
	6-311++G(2d,2p)	−2016.35258820	−9.958	3.035	176.8
H ₂ S–[C ₂ mim] ⁺	6-311+G(d)	−744.041520141	−19.16	2.744	93.82
	6-311++G(2d,2p)	−744.083507691	−17.82	2.748	93.24
CO ₂ –[C ₂ mim] ⁺	6-311+G(d)	−533.272012803	−11.01	2.300	179.98
	6-311++G(2d,2p)	−533.304590604	−9.51	2.334	179.97

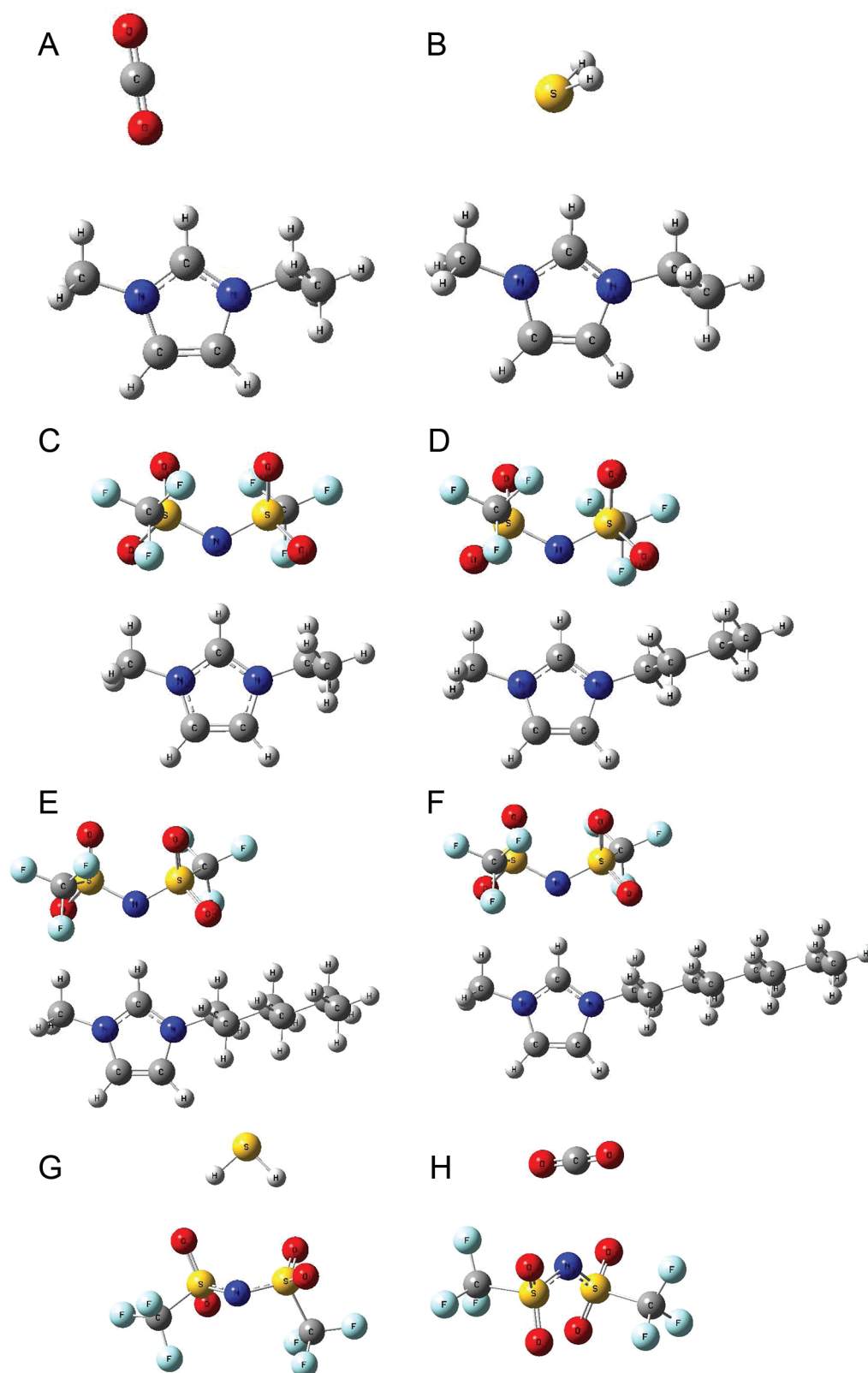


Figure 10. Minimum energy structures for the dimers studied in this work: (a) $\text{CO}_2/[\text{C}_2\text{mim}]^+$; (b) $\text{H}_2\text{S}/[\text{C}_2\text{mim}]^+$; (c) $[\text{C}_2\text{mim}][\text{Tf}_2\text{N}]^-$; (d) $[\text{C}_4\text{mim}][\text{Tf}_2\text{N}]^-$; (e) $[\text{C}_6\text{mim}][\text{Tf}_2\text{N}]^-$; (f) $[\text{C}_8\text{mim}][\text{Tf}_2\text{N}]^-$; (g) $\text{H}_2\text{S}/[\text{Tf}_2\text{N}]^-$; (h) $\text{CO}_2/[\text{Tf}_2\text{N}]^-$.

anion and cation (Table 11). Also it can be seen that as the size of the alkyl substituent of the imidazolium ring increases no folding results and it chooses the linear configuration. Since ab initio calculations on the species are performed in the isolated

gas phase state, we certainly cannot conclude that chain folding does not occur in the condensed liquid phase, where the multiple interactions with other molecules surrounding each molecule and reduction in volume are important and molecular

simulation studies need to be performed to clarify and fix the problem. From Table 11, it can be deduced that the interaction energy, E_{binding} for anion–cation complexes, decreases from $[\text{C}_2\text{mim}][\text{Tf}_2\text{N}]$ to $[\text{C}_6\text{mim}][\text{Tf}_2\text{N}]$ and then increases for $[\text{C}_8\text{mim}][\text{Tf}_2\text{N}]$ by using the 6-311+G(d) basis set. However, a decreasing trend in interaction energy can be observed from $[\text{C}_2\text{mim}][\text{Tf}_2\text{N}]$ to $[\text{C}_8\text{mim}][\text{Tf}_2\text{N}]$ when using the 6-311++G(2d,2p) basis set. Both basis sets indicate that the interaction of H_2S with the anion and cation of the ionic liquid is more energetic than those of CO_2 . This observation is pronounced by the more polarized and diffused basis set 6-311++G(2d,2p), which implies that the interaction energy of H_2S with the $[\text{Tf}_2\text{N}]^-$ anion is of the order of traditional hydrogen bond and is about three times stronger than that of CO_2 with $[\text{Tf}_2\text{N}]^-$. However, the type of the hydrogen bond does not show strong directionality.⁵⁸ The hydrogen atoms of the H_2S molecule are not directed toward the most electronegative fluorine atoms. Instead, they are directed toward the less electronegative nitrogen atom of the $[\text{Tf}_2\text{N}]^-$ anion. The gas phase ab initio quantum chemical calculations using geometry optimizations at both the B3LYP/CEP-121G(d,p) and the MP2/121G(d,p) levels of theory on H_2S -anion complexes made by Pomelli et al.¹⁷ as well as those performed on CO_2 -anion complexes at the B3LYP/6-311+G* and MP2/6-311+G* by Bhargava and Balasubramanian,⁵⁹ qualitatively confirm this same conclusion. The interaction energies for H_2S - $[\text{Tf}_2\text{N}]^-$ complex are -5.11 and -7.61 kcal·mol⁻¹,¹⁷ respectively (interaction energy is in the order of hydrogen bond), while the corresponding values for the CO_2 - $[\text{Tf}_2\text{N}]^-$ complex are -2.37 and -2.80 kcal·mol⁻¹ at the B3LYP and MP2 levels of theory, respectively.⁵⁹ Furthermore, Bhargava and Balasubramanian⁵⁹ concluded that the optimized structures of CO_2 -anion complexes are dominated by Lewis acid–base interactions, with the carbon atom of CO_2 as the electron acceptor (acid) and the anion as the donor (base). From the above discussions, we can conclude that the stronger interaction of H_2S with the $[\text{Tf}_2\text{N}]^-$ anion with respect to CO_2 is responsible for the higher solubility of H_2S in $[\text{C}_n\text{mim}][\text{Tf}_2\text{N}]$ ionic liquids. Brennecke and co-workers^{60,61} showed that the solubility of gases in ionic liquids correlate well with gas polarizability, that is, the solubility increases as the gas polarizability increases. Applying this conclusion here it can be seen that H_2S with a higher dipole polarizability, $\alpha_{\text{d}} = 3.95 \times 10^{-24}$ cm³ relative to CO_2 , $\alpha_{\text{d}} = 2.911 \times 10^{-24}$ cm³ shows a higher solubility in $[\text{C}_n\text{mim}][\text{Tf}_2\text{N}]$ ionic liquids too. The optimized structures corresponding to the B3LYP/6-311++G(2d,2p) level of theory for the H_2S - $[\text{Tf}_2\text{N}]^-$ and CO_2 - $[\text{Tf}_2\text{N}]^-$ complexes are shown in Figures 10g and h, respectively. In the case of the H_2S - $[\text{Tf}_2\text{N}]^-$ complex, the hydrogen atoms of H_2S are directed toward the two oxygen atoms of the $[\text{Tf}_2\text{N}]^-$ anion with a 1.6° decrease in H–S–H angle and about 0.004 Å increase in H–S bond length. This same orientation of interaction with less angle contraction can be observed when using the B3LYP/6-311+G(d) level of theory. The H–S–H angle in a free H_2S molecule is computed to be 92.70° at the B3LYP/6-311++G(2d,2p) level of theory. In the case of CO_2 - $[\text{Tf}_2\text{N}]^-$ complex, Figure 10h shows that the carbon atom of the CO_2 molecule is aligned between the nitrogen and one of the oxygen atoms of the $[\text{Tf}_2\text{N}]^-$ anion with the oxygen atoms of CO_2 positioned in the farthest distance from the N and O atoms of the $[\text{Tf}_2\text{N}]^-$ anion so as to minimize the repulsive interaction of the oxygen atoms with the anion. The distortion of CO_2 from a linear geometry upon complexation is 3.2° and 3.7° when using the 6-311+

+G(2d,2p) and 6-311+G(d) basis sets, respectively. Also it can be observed that the interaction of both CO_2 and H_2S with the prototype cation $[\text{C}_2\text{mim}]^+$ is weaker than that of $[\text{Tf}_2\text{N}]^-$ anion being stronger in the case of H_2S - $[\text{C}_2\text{mim}]^+$ complex relative to the CO_2 - $[\text{C}_2\text{mim}]^+$ complex.

There is a surprisingly excellent linear correlation (with $R^2 > 0.9999$) between the absolute value of the energies of $[\text{C}_n\text{mim}][\text{Tf}_2\text{N}]$ complexes from ab initio calculations and correlated Henry's law constants generated by eqs 17 and 18 for the solubility of both CO_2 and H_2S gases in $[\text{C}_n\text{mim}][\text{Tf}_2\text{N}]$ ILs at each specified temperature. Equation 35 shows this correlation

$$K_{\text{h},x}^{(0)}(T) = a(T)(|E_{\text{complex}}/\text{Hartree}|) + b(T) \quad (35)$$

where $a(T)$ and $b(T)$ are linear functions of temperature in kelvin

$$a(T) = -0.00017295(T/K) + 0.04701364 \quad \text{CO}_2 \quad (36a)$$

$$b(T) = 0.44005306(T/K) - 117.91173103 \quad \text{CO}_2 \quad (36b)$$

$$a(T) = -0.00005940(T/K) + 0.01582844 \quad \text{H}_2\text{S} \quad (36c)$$

$$b(T) = 0.16433102(T/K) - 43.60051328 \quad \text{H}_2\text{S} \quad (36d)$$

This linear correlation between theoretically obtained absolute energies of $[\text{C}_n\text{mim}][\text{Tf}_2\text{N}]$ complexes on one hand and relations obtained from the experimental data on the other hand further justifies the assumption that the solubility of acid gases CO_2 and H_2S in $[\text{C}_n\text{mim}][\text{Tf}_2\text{N}]$ ILs increases as the size of the alkyl chain of the imidazolium ring in the cation increases by decreasing the density or equivalent increase in free volume of the IL. Furthermore, it provides theoretical support for the experimental data reported in this work. Thus, by computing the geometry optimized ab initio energy of an isolated $[\text{C}_n\text{mim}][\text{Tf}_2\text{N}]$ complex at B3LYP/6-311++G(2d,2p) level of theory using eqs 35 and 36, one can obtain Henry's law constant in the limit of zero pressure at the specified temperature, T , for dissolution of carbon dioxide or hydrogen sulfide in $[\text{C}_n\text{mim}][\text{Tf}_2\text{N}]$ ionic liquids.

CONCLUSIONS

New experimental data for the solubility and thermodynamic functions of solutions of carbon dioxide and hydrogen sulfide gases in the ionic liquid 1-octyl-3-imidazolium bis-(trifluoromethyl)sulfonylimide, not previously reported in the literature, have been measured and presented in this work. The solubility of H_2S is higher than that of CO_2 in $[\text{C}_8\text{mim}][\text{Tf}_2\text{N}]$. The solubility of both gases in the IL studied in this work is of a physical nature. It has been shown that the solubility of both CO_2 and H_2S gases in $[\text{C}_n\text{mim}][\text{Tf}_2\text{N}]$ ILs increases by increasing the number of carbons in the alkyl substituent of the methylimidazolium cation ring. The solubility data for the $\text{CO}_2/\text{H}_2\text{S}/[\text{C}_8\text{mim}][\text{Tf}_2\text{N}]$ ternary system can best be correlated by means of the generic Redlich–Kwong cubic equation of state proposed for gas/ionic liquid systems. The addition of the ionic liquid makes feasible the separation of CO_2 and H_2S from each other especially at high temperatures where the traditional distillation procedure fails to work at these conditions. Ab initio quantum chemical calculations provide qualitatively useful clues to understand the nature of the

solubility of CO₂ and H₂S acid gases in [C_nmim][Tf₂N] ionic liquids. Useful relations were presented in this work to calculate the Henry's law constants for the solubility of acid gases in [C_nmim][Tf₂N] ionic liquids by performing only quantum chemical calculations on [C_nmim][Tf₂N] isolated complexes.

AUTHOR INFORMATION

Corresponding Author

*E-mail: jaliliah@ripi.ir, jaliliah@yahoo.com. Tel.: 98-21-48252466; fax: 98-21-44739716.

Notes

The authors declare no competing financial interest.

ACKNOWLEDGMENTS

We are thankful to the research council of the Research Institute of Petroleum Industry (RIPI) and also to the Research and Development of the National Iranian Oil Company (NIOC) for their support of this work. The corresponding author also gratefully acknowledges Prof. Gerd Maurer for his kind guidance in correlating experimental data.

REFERENCES

- (1) *Ionic Liquids in Synthesis*; Wassercheid, P., Welton, T., Eds.; Wiley-VCH: Weinheim, Germany, 2002.
- (2) Kohl, A. L.; Nielsen, R. B. *Gas Purification*, 5th ed.; Gulf Publishing Company: Houston, TX, 1997.
- (3) Camper, D.; Bara, J. E.; Gin, D. L.; Noble, R. D. *Ind. Eng. Chem. Res.* **2008**, *47*, 8496–8498.
- (4) Galán Sánchez, L. M.; Meindersma, G. W.; de Haan, A. B. *Trans. IChemE, Part A, Chem. Eng. Res. Des.* **2007**, *85*, 31–39.
- (5) Bates, E. D.; Mayton, R. D.; Ntai, I.; Davis, J. H. *J. Am. Chem. Soc.* **2002**, *124*, 926–927.
- (6) Goodrich, B. F.; de la Fuente, J. C.; Gurkan, B. E.; Zadigian, D. J.; Price, E. A.; Huang, Y.; Brennecke, J. F. *Ind. Eng. Chem. Res.* **2011**, *50*, 111–118.
- (7) Gurkan, B. E.; de la Fuente, J. C.; Mindrup, E. M.; Ficke, L. E.; Goodrich, B. F.; Price, E. A.; Schneider, W. F.; Brennecke, J. F. *J. Am. Chem. Soc.* **2010**, *132*, 2116–2117.
- (8) Blanchard, L. A.; Gu, Z.; Brennecke, J. F. *J. Phys. Chem. B* **2001**, *105*, 2437–2444.
- (9) Aki, S. N. V. K.; Mellein, B. R.; Saurer, E. M.; Brennecke, J. F. *J. Phys. Chem. B* **2004**, *108*, 20355–20365.
- (10) Baltus, R. E.; Culbertson, B. H.; Dai, S.; Luo, H.; DePaoli, D. W. *J. Phys. Chem. B* **2004**, *108*, 721–727.
- (11) Chen, Y.; Zhang, S.; Yuan, X.; Zhang, Y.; Zhang, X.; Dai, W.; Mori, R. *Thermochim. Acta* **2006**, *441*, 42–44.
- (12) Zhang, J.; Zhang, Q.; Qiao, B.; Deng, Y. *J. Chem. Eng. Data* **2007**, *52*, 2277–2283.
- (13) Gutowski, K. I.; Shariati, A.; Peters, C. J. *J. Supercrit. Fluids* **2006**, *39*, 187–191.
- (14) Shin, E.-K.; Lee, B.-C.; Lim, J. S. *J. Supercrit. Fluids* **2008**, *45*, 282–292.
- (15) Shin, E.-K.; Lee, B.-C. *J. Chem. Eng. Data* **2008**, *53*, 2728–2734.
- (16) Jou, F.-Y.; Mather, A. E. *Int. J. Thermophys.* **2007**, *28*, 490–495.
- (17) Pomelli, C. S.; Chiappe, C.; Vidis, A.; Laurenczy, G.; Dyson, P. J. *J. Phys. Chem. B* **2007**, *111*, 13014–13019.
- (18) Heintz, Y. J.; Sehabiague, L.; Morsi, B. I.; Jones, K. L.; Luebke, D. R.; Pennline, H. W. *Energy Fuels* **2009**, *23*, 4822–4830.
- (19) Shiflett, M. B.; Yokozeki, A. *Fluid Phase Equilib.* **2010**, *294*, 105–113.
- (20) Jalili, A. H.; Rahmati-Rostami, M.; Ghotbi, C.; Hosseini-Jenab, M.; Ahmadi, A. N. *J. Chem. Eng. Data* **2009**, *54*, 1844–1849.
- (21) Rahmati-Rostami, M.; Ghotbi, C.; Hosseini-Jenab, M.; Ahmadi, A. N.; Jalili, A. H. *J. Chem. Thermodyn.* **2009**, *41*, 1052–1055.
- (22) Shokouhi, M.; Adibi, M.; Jalili, A. H.; Hosseini-Jenab, M.; Mehdizadeh, A. *J. Chem. Eng. Data* **2010**, *55*, 1663–1668.
- (23) Jalili, A. H.; Mehdizadeh, A.; Shokouhi, M.; Ahmadi, A. N.; Hosseini-Jenab, M.; Fateminassab, F. *J. Chem. Thermodyn.* **2010**, *42*, 1298–1303.
- (24) Sakhaeinia, H.; Taghikhani, V.; Jalili, A. H.; Mehdizadeh, A.; Safekordi, A. A. *Fluid Phase Equilib.* **2010**, *298*, 303–309.
- (25) Sakhaeinia, H.; Jalili, A. H.; Taghikhani, V.; Safekordi, A. A. *J. Chem. Eng. Data* **2010**, *55*, 5839–5845.
- (26) Pitzer, K. S. *Thermodynamics of Electrolytes. I. Theoretical Basis and General Equations.* *J. Phys. Chem.* **1973**, *77*, 268–277.
- (27) *Activity Coefficients in Electrolyte Solutions*; Pitzer, K. S., Ed.; CRC Press: Boca Raton, FL, 1991.
- (28) Shiflett, M. B.; Yokozeki, A. *Ind. Eng. Chem. Res.* **2005**, *44*, 4453–4464.
- (29) Shiflett, M. B.; Yokozeki, A. *J. Chem. Eng. Data* **2006**, *51*, 1931–1939.
- (30) Shiflett, M. B.; Yokozeki, A. *J. Phys. Chem. B* **2007**, *111*, 2070–2074.
- (31) Yokozeki, A.; Shiflett, M. B.; Junk, C. P.; Grieco, L. M.; Foo, T. *J. Phys. Chem. B* **2008**, *112*, 16654–16663.
- (32) Krichevsky, I. R.; Kasarnovsky, J. S. *J. Am. Chem. Soc.* **1935**, *57*, 2168–2171.
- (33) Huddleston, J. G.; Rogers, R. D. *Chem. Commun.* **1998**, 1765–1766.
- (34) *NIST Scientific and Technical Databases, Thermophysical Properties of Fluid Systems.* <http://webbook.nist.gov/chemistry/fluid/> (accessed March 2011).
- (35) Huber, M. L. *Thermophysical Properties of Hydrocarbon Mixtures Database (SUPERTRAPP)*, NIST Standard Reference Database 4, Version 3.2; NIST: Gaithersburg, MD, 2007.
- (36) Prausnitz, J. M.; Lichtenthaler, R. N.; Azevedo, E. G. *Molecular Thermodynamics of Fluid Phase Equilibria*, 3rd ed.; Prentice Hall: Englewood Cliffs, NJ, 1999.
- (37) Kumelan, J.; Pérez-Salado Kamps, Á.; Tuma, D.; Yokozeki, A.; Shiflett, M. B.; Maurer, G. *J. Phys. Chem. B* **2008**, *112*, 3040–3047.
- (38) Kumelan, J.; Pérez-Salado Kamps, Á.; Tuma, D.; Maurer, G. *J. Chem. Thermodyn.* **2006**, *38*, 1396–1401.
- (39) Kumelan, J.; Tuma, D.; Maurer, G. *Fluid Phase Equilib.* **2011**, *311*, 9–16.
- (40) Yokozeki, A. *Int. J. Thermophys.* **2001**, *22*, 1057–1071.
- (41) Frisch, M. J.; Trucks, G. W.; Schlegel, H. B.; Scuseria, G. E.; Robb, M. A.; Cheeseman, J. R.; Montgomery, J. A., Jr.; Vreven, T.; Kudin, K. N.; Burant, J. C.; et al. *Gaussian 03, Revision C.02*; Gaussian, Inc.: Wallingford, CT, 2004.
- (42) Ransil, B. J. *J. Chem. Phys.* **1961**, *34*, 2109–2118.
- (43) Boys, S. F.; Bernardi, F. *Mol. Phys.* **1970**, *19*, 553–566.
- (44) Krummen, M.; Wasserscheid, P.; Gmehling, J. *J. Chem. Eng. Data* **2002**, *47*, 1411–1417.
- (45) Kato, R.; Gmehling, J. *J. Chem. Thermodyn.* **2005**, *37*, 603–619.
- (46) Kazarian, S. G.; Briscoe, B. J.; Welton, T. *Chem. Commun.* **2000**, 2047–2048.
- (47) Anderson, J. L.; Dixon, J. K.; Brennecke, J. F. *Acc. Chem. Res.* **2007**, *40*, 1208–1216.
- (48) Bara, J. E.; Carlisle, T. K.; Gabriel, C. J.; Camper, D.; Finotello, A.; Gin, D. L.; Noble, R. D. *Ind. Eng. Chem. Res.* **2009**, *48*, 2739–2751.
- (49) Camper, D.; Scovazzo, P.; Koval, C.; Noble, R. D. *Ind. Eng. Chem. Res.* **2004**, *43*, 3049–3054.
- (50) Finotello, A.; Bara, J. E.; Narayan, S.; Camper, D.; Noble, R. D. *J. Phys. Chem. B* **2008**, *112*, 2335–2339.
- (51) Jacquemin, J.; Husson, P.; Majer, V.; Costa Gomes, M. F. *Fluid Phase Equilib.* **2006**, *240*, 87–95.
- (52) Poling, B. E.; Prausnitz, J. M.; O'Connell, J. P. *The Properties of Gases and Liquids*, 5th ed.; McGraw-Hill: New York, 2001.
- (53) Valderrama, J. O.; Robles, P. A. *Ind. Eng. Chem. Res.* **2007**, *46*, 1338–1344.
- (54) Valderrama, J. O.; Sanga, W. W.; Lazzus, J. A. *Ind. Eng. Chem. Res.* **2008**, *47*, 1318–1330.
- (55) Shen, C.; Li, C.; Li, X.; Lu, Y.; Muhammad, Y. *Chem. Eng. Sci.* **2011**, *66*, 2690–2698.
- (56) Yokozeki, A.; Shiflett, M. B. *Appl. Energy* **2007**, *84*, 351–361.

(57) Yokozeki, A.; Shiflett, M. B. *Ind. Eng. Chem. Res.* **2008**, *47*, 8389–8395.

(58) Tsuzuki, S.; Tokuda, H.; Mikami, M. *Phys. Chem. Chem. Phys.* **2007**, *9*, 4780–4784.

(59) Bhargava, B. L.; Balasubramanian, S. *Chem. Phys. Lett.* **2007**, *444*, 242–246.

(60) Anthony, J. L.; Maginn, E. J.; Brennecke, J. F. *J. Phys. Chem. B* **2002**, *106*, 7315–7320.

(61) Anthony, J. L.; Anderson, J. L.; Maginn, E. J.; Brennecke, J. F. *J. Phys. Chem. B* **2005**, *109*, 6366–6374.

(62) The Henry's law constants are obtained from the PTx data for the solubility of CO_2 in $[\text{C}_2\text{mim}][\text{Tf}_2\text{N}]$, the manuscript of which is under preparation.